

# Influence of Hurricane Wind Field Variability on Real-time Forecast Simulations of the Coastal Environment

Rey, A.J.M.<sup>1</sup>, Mulligan, R.P.<sup>1</sup>

<sup>1</sup>Department of Civil Engineering, Queen's University, 58 University Ave, Kingston, ON, K7L 3N9,  
Canada

## Key Points:

- A novel high-resolution regional modelling system for real-time coastal forecasts of surface waves, currents, and water levels is developed.
- Forcing input from different atmospheric model hindcasts and forecasts are compared to assess the accuracy of output results.
- Model results are quantitatively in very good agreement with observations across coastal NC during Hurricane Dorian in September 2019.

## Abstract

Dynamic conditions occur in the coastal ocean during severe storms. Forecasting these conditions is challenging, and large-scale numerical models require significant computing power. In this paper, we describe a real-time modelling system (DUNEX-RT), developed in support of the DURING Nearshore Event eXperiment (DUNEX) in North Carolina, USA. The model is run with wave, current, and water level boundary conditions from larger-scale models, and provides 36-hour forecasts of significant wave height, depth-averaged velocity, and water levels every 6-hours using Delft3D-SWAN. Observations and forecasts run at different times are compared and communicated via an interactive website to verify model performance in real-time and to visualize uncertainty from changing inputs. Here, we evaluate model sensitivity to inputs from different atmospheric hindcasts and forecasts for Hurricane Dorian (2019). The real-time model had relatively low errors across the system, indicating that this novel approach can be applied to forecast other areas of the coastal ocean.

## Plain Language Summary

Dynamically changing wave and current conditions occur in the coastal ocean during severe storm events, including hurricanes. Forecasting these conditions is challenging, and existing large-scale numerical models require significant computing power and can have limitations. In this paper, we describe a real-time modelling system of coastal North Carolina, USA. This model provides forecasts of the waves, currents and water levels every 6-hours. The model results are compared with real-time observations and communicated on an interactive website to allow users to visualize differences in results based on winds forecast at different times. Detailed results are presented for Hurricane Dorian in September 2019, and the model had relatively low errors at many sites across the system. This suggests that this novel high-resolution regional modelling approach can be applied to forecast conditions in other areas of the coastal ocean.

## 1 Introduction

Tropical cyclones are a significant and increasing natural hazard for human life and infrastructure along many coastlines throughout the world. Atlantic Ocean hurricanes deliver powerful conditions to the east and gulf coasts of North America annually, and are the most destructive natural disaster in the United States (Grinsted et al., 2019). The frequency and intensity of these storms is projected to increase with future climate warming and longer storm formation periods (Knutson et al., 2010). During these storms large waves, high storm surge, and strong currents can combine to create a multi-hazard marine environment, making understanding the impacts of these events in coastal areas a vital research area (Mulligan and Hanson, 2016). Presently, atmospheric models can be used to forecast wind conditions during a storm, and large-scale ocean models can provide predictions of surface waves, water levels, and currents. However, these forecasts lack the high resolution needed to resolve local conditions and smaller scale features, preventing their application in coastal and nearshore areas. Significant computational resources are also typically required for simulations over large domains, further limiting their application (Bilskie et al., 2019).

Atmospheric modelling has progressed dramatically over the last decade in conjunction with the availability of high performance computing resources, however, translating these advances into hurricane impacts on coastal ocean environments remains an active research area. Most research has focused on hurricane storm surge, for example Bennett et al. (2018) used a detailed wind hindcast with significant spatial variability to simulate inundation and overwash in a back-barrier estuary during Hurricane Sandy. Thomas et al. (2019) compared multiple wind hindcast models with a large observational dataset to investigate the effects of storm speed and timing on water levels. The importance of including wave effects on coastal circulation during hurricanes has also been emphasized in several studies (eg. Mulligan et al. 2008). Sheng et al. (2010) applied a wave-current model to the Outer Banks of North Carolina (NC) and Chesapeake Bay during Hurricane Isabel in 2003, and found that including waves improved the results. This finding is shared by Drost et al. (2017), who also highlighted the fact that bottom friction is a priority area for research as a key calibration parameter in coastal models.

Increasing our understanding of risks posed by major storms has been identified as an important area for investigation by the nearshore research community (Elko et al., 2015). This includes improving numerical models of the fundamental coastal ocean processes that

contribute to damage during storms, including waves (Drost et al., 2017; Bennett and Mulligan, 2017), erosion (Gittman et al., 2014; Xie et al., 2018), and storm surge (Powell et al., 2010; Dietrich et al., 2018). Despite these advances, the nearshore research community has recently united to determine remaining research gaps and modelling limitations in the response of coastal environments to storms (Elko et al., 2019). The extreme spatial and temporal variability of hurricanes requires model validation at many sites, and collaboration is necessary to facilitate sensor deployment over a large area. The DURING Nearshore Event eXperiment (DUNEX) was proposed by the US Coastal Research Program (Cialone et al., 2019) to support this by providing a platform for research collaboration. Accurate and high resolution real-time coastal surface forecasts provide a useful way of planning and optimizing deployment sites immediately before a major storm event.

Recognizing the need for coastal forecasts to incorporate relevant processes and communicate uncertainty in predicted storm tracks and wind fields, a real-time forecast system was developed for coastal NC using Delft3D-SWAN. In this study, the accuracy of different hindcast and forecast wind models are compared against observations across a range of coastal environments including the continental shelf, barrier islands, inlets, and estuaries. This paper describes the development, validation, and real-time communication of the results for Hurricane Dorian in 2019.

## 2 Methods

### 2.1 Hurricane Dorian

Hurricane Dorian caused major destruction in the mid-Atlantic in August and September of 2019. Dorian made landfall in the Bahamas on September 1 as a category 5 Hurricane on the Saffir-Simpson scale, and was the strongest recorded storm to hit the island (Lixion and Cangialosi, 2019; Royal Meteorological Society, 2019). With 82 m/s sustained wind speeds and a peak storm surge of 7 m, Dorian resulted in 69 fatalities and widespread devastation throughout the Bahamas (UNICEF, 2019). After moving along the US east coast, Dorian made landfall again on September 6 at Cape Hatteras, NC, as a category 1 storm with 33 m/s sustained winds (Cangialosi, 2019). Widespread wind damage, offshore waves of over 6 m, up to 200 mm of rain, and significant flooding were reported, producing mandatory evacuations, impacting 681 homes, and causing 3 deaths (FEMA, 2019; National Weather Service, 2019). The post tropical cyclone continued northward and impacted Hal-



ifax, Nova Scotia, Canada, on September 7 (Beven, 2019). In this study, we investigate the storm conditions as it impacted eastern NC.

## 2.2 Observations

Observations are obtained from 18 wind anemometers, 21 water level gauges, 8 wave buoys, and 4 current sensors at sites shown in Figure 1. Water level measurements are obtained from the National Oceanic and Atmospheric Administration (NOAA), United States Geological Survey (USGS), US Army Corps of Engineers (USACE), and the National Weather Service (NWS) (Herzmann et al., 2004). Wave observations are sourced from the National Data Buoy Centre (NDBC) and the Coastal Data Information Program (CDIP) (Flick et al., 1993). Current velocity observations are collected by the USACE Field Research Facility (FRF). Real-time observations during Hurricane Dorian were saved every 6 hours and communicated together with the model results via the web interface. A complete list of all observation sources is provided in Supporting Information Table A1. Observations from across the system are used to statistically quantify model errors and are discussed in Section 3.

## 2.3 Numerical Model

Numerical models are commonly applied to help understand coastal processes during storms; however, relatively few studies have analyzed the performance of coastal models in a real-time forecast configuration. Mulligan et al. (2011) accurately predicted wave conditions in a small and semi-protected bay using the SWAN wave model (Booij et al., 1999) with boundary wave inputs from WaveWatch III (Chawla et al., 2013). Olabarrieta et al. (2011) applied the COAWST modelling system with WaveWatch III results at the boundaries to examine a hurricane. The NOAA Coastal Emergency Risks Assessment (ERA) (Blanton et al., 2012) provides a web accessible 7-day forecast of water levels along the east coast of North America; however, currents are not reported in real-time. Dresback et al. (2013) found good model agreement with observations but noted the importance of accurate atmospheric forcing, a finding also emphasized by Cyriac et al. (2018) during a hurricane. The USGS Total Water Level and Coastal Change Forecast Viewer provides inundation predictions along selected coastlines, but is limited to nearshore water levels (Aretxabaleta et al., 2019). While currents are included in the Navy Coastal Ocean Model (NCOM), resolution is limited ( $> 3.7$  km) and waves are not included (Martin et al., 2009). Paramygin et al. (2017)

applied the CH3D model nested in a large-scale ADCIRC grid and identified that enhanced resolution in coastal zones is possible using this approach; however, the large-scale grid simulations require significant computational time. Recently, Dietrich et al. (2018) found that atmospheric forecasts produce more accurate coastal forecasts compared to parametric hurricane wind models. This was also identified by Garzon et al. (2018) in Chesapeake Bay, with more accurate water levels when using the NOAA North American Mesoscale Model (NAM) compared to parametric winds. An 84-hour forecast for the northeast Atlantic is produced using SWAN+ADCIRC; however, the large domains requires significant computational resources (Ferreira, 2017). High computational demands can be necessary to simulate large domains at high resolution, for example, requiring 1,000 - 3,000 cores to complete a 5-day simulation within a 2-hour forecast time frame (Bilskie et al., 2019).

### 2.3.1 *DUNEX-RT Set-up*

The real-time (RT) model developed is from here on referred to as DUNEX-RT, and the domain was selected to cover the DUNEX project area, maximize coverage of different coastal environments, and include relevant observation points. Shown in Figure 1, the domain covers the Albemarle-Pamlico Estuarine System (APES), including back-barrier estuaries, inlets, barrier islands, and the coastal ocean across the continental shelf. Delft3D (Lesser et al., 2004) solves the Navier-Stokes horizontal momentum equations, and is capable of simulating water levels and currents forced by both spatially varying meteorology and boundary inputs (currents and water levels). Waves, including wave-current interactions, are coupled through SWAN (Booij et al., 1999), a third generation shallow water spectral wave model which predicts wave generation, propagation, and dissipation. Delft3D-SWAN has been applied successfully to this environment, notably by Mulligan et al. (2015) to model Hurricane Irene, by Clunies et al. (2017) to investigate waves and storm surge, and by Mulligan et al. (2019) to study long-term estuarine response to changing morphology and sea-level rise. In the present study, a 2D structured grid is used, with the flow grid resolution varying from 100 m to 400 m, and the wave grid resolution varying between 250 m and 1000 m. Bathymetry was obtained from the NOAA coastal relief model (CRM), with a resolution of approximately 30 m (NOAA National Centers for Environmental Information, 2016). The DUNEX-RT system operates every 6 hours by producing 36-hour forecasts that are “hot-started” using results from the previous 6-hour forecast, and computations are performed with a 15-second time step. DUNEX-RT is run on 16 Intel Xeon processors with 32 GB

of RAM and takes 5 hours for simulation and 1 hour for processing. All parameters are the model defaults except for bed roughness, which was decreased by adjusting the Chézy bottom roughness parameter (inversely proportional to the bottom drag coefficient) from  $C_z = 65$  to  $95 \text{ m}^{1/2} \text{ s}^{-1}$ , similar to the approach used by Drost et al. (2017). This adjustment increases predicted current velocities at two offshore stations (*F6*, *F11*), reducing the Root-Mean-Square-Difference (RMSD) depth-averaged velocity during the 36-hour crossing of Hurricane Dorian by 10% and 19% at these two sites. This change has negligible impacts on the accuracy of wave and water level results elsewhere in the domain, and the remainder of this paper focuses on the sensitivity to different input wind conditions.

### 2.3.2 Forcing from Large-scale Models

To minimize computational requirements and enable forecast runs to be completed in under 6 hours, the high resolution grid is forced at the boundaries from large-scale ocean forecast models. Riemann type boundaries (Stelling, 1983) are used in 183 segments at 5 km intervals for depth-averaged currents and water levels. Multiple sources (summarized in Table 1) are used for the boundary conditions. Water level forecasts are provided by the Extratropical Surge and Tide Operational Forecast System (ESTOFS), a North Atlantic surge and tide model (Funakoshi et al., 2012). NCOM provides currents (Martin et al., 2009), which are depth-averaged to approximate boundary flows following the method described by Edwards et al. (2012). The NOAA multi-grid WaveWatch III model (Chawla et al., 2013), forecasts significant wave height, peak period, and mean wave directions that are applied to DUNEX-RT in 36 ocean boundary segments at 25 km intervals. Hindcast simulations were also performed, using hindcast wind fields, to compare with the forecast predictions. These hindcast simulations used observations at the boundaries, including water levels at the FRF and the Beaufort Marine Lab (Figure 1 *FP* and *BF*), as well as 2D wave spectra from four directional wave buoys (Figure 1 *OB*, *DS*, *VB*, and *CH*).

Atmospheric forcing (pressure and winds), comes from several global and mesoscale models summarized in Table 1. Analysis products from the Global Forecast System (GFS), North American Mesoscale Forecast System (NAM), and Rapid Refresh (RAP) models were used to hindcast the storm (Yang et al., 2006; Rogers et al., 2009; Benjamin et al., 2016), in addition to reanalysis data from the Climate Forecast System (CFSv2) and the European Reanalysis (ERA5) (Saha et al., 2010; Hersbach and Dee, 2016; Copernicus Climate Change Service (C3S), 2017). Atmospheric data is linearly interpolated to a 2.5 km input

grid. Forecasts from the Regional Deterministic Prediction System (RDPS; from Mai et al. (2019)), and the High Resolution Rapid Refresh Model (HRRR; from Blaylock et al. (2017) and Agrawal et al. (2019)) are used in both hindcast (zero-hour initialization) and forecast configurations and are described in Caron et al. (2015) and Smith et al. (2008) respectively.

### 3 Results and Discussion

A visualization of the wind fields described in Table 1 at 18:00 UTC on September 6 are shown in Figure 2 with wind magnitude observations shown in coloured circles. Notable differences exist between wind fields, causing significant changes in hydrodynamic predictions. Overall hurricane shape and strength is similar; however, the size and location of the eye varies considerably. Offshore at the Virginia Beach buoy (Figure 1 *VB*), the HRRR and RAP winds were from the northeast (Figure 2 a,d), while the RDPS winds were from the northwest (Figure 2 b) at the same time, and all models are different in wind speed. Resolution differences between models are apparent, with the lower resolution CFSv2 (27 km), GFS (27 km), and ERA5 (30 km) models failing to resolve local variations in wind speeds compared to the high resolution RAP (13 km), HRRR (3.5 km), and RDPS (2.5 km) models during this storm with high spatial variability in winds. Differences between wind forecasts at a specified time (e.g. 18:00 UTC) are evident between runs initialized at 18:00 UTC (18:00 UTC start, zero-hour (00Z) forecast), and runs that were initialized 18 hours prior (00:00 UTC start, 18-hour (18Z) forecast) shown in Figure 2 a,h for the HRRR model and Figure 2 b,i for the RDPS model. While the eye was in a similar location for both HRRR runs, a stronger northern wind was forecasted along the coast during the 00Z run compared to the 18Z run, producing important differences in the forecasted currents. For example, currents at site *F11* were predicted to be 1.4 m/s at 18:00 UTC from the HRRR wind field forecast initialized at 00:00 UTC, compared to 0.6 m/s from forecast started at 18:00 UTC (Supporting Information Figure A5). Variations between RDPS forecasts are also evident, with eye moving approximately 150 km farther offshore between the 00:00 UTC and 18:00 UTC runs.

Modified Taylor diagrams (Taylor, 2001; Elvidge et al., 2014) are a useful way to visualize model performance by comparing 3 statistics on a single plot. The results of DUNEX-RT after using 7 hindcasts and 2 forecasts as input over a 36-hour period (September 6 00:00 UTC to September 7 12:00 UTC) are shown at 9 selected sites across the system for 3 difference parameters ( $\eta, Hs, |u|$ ) in Figure 3. These diagrams display the correlation coefficients

(R) along the azimuthal angle, the model standard deviations ( $\sigma_m$ ) are normalized against observed standard deviations ( $\sigma_o$ ) and are shown along the radial axis ( $\sigma^* = \sigma_m/\sigma_o$ ). In addition, the Centred-Root-Mean-Square-Differences (CRMSD, bias corrected RMSD) are radially distributed from the observation point at  $\sigma^* = 1$  and  $R = 1$ . Using this approach, model results with higher agreement with observations are plotted closer to the location of the normalized observation point. The overall statistics indicate that the zero-hour HRRR provided the best hindcast results (RMSD = 0.16 m for  $\eta$ ; 0.42 m for  $Hs$ ; and 0.23 m/s for  $|u|$ ), with the zero-hour RDPS model similarly accurate (RMSD = 0.21 m for  $\eta$ ; 0.61 m for  $Hs$ ; and 0.17 m/s for  $|u|$ ). Consequently, the HRRR and RDPS models were evaluated in a forecast configuration, with slightly more accurate results from HRRR (RMSD = 0.16 m for  $\eta$ ; 0.56 m for  $Hs$ ; and 0.25 m/s for  $|u|$ ) than RDPS (RMSD = 0.21 m for  $\eta$ ; 0.66 m for  $Hs$ ; and 0.20 m/s for  $|u|$ ). Despite the overall higher accuracy of the HRRR forecast, more accurate southward winds at the FRF sites in the RDPS forecasts produced improved depth-averaged velocity forecasts at the observed sites in the coastal ocean ( $F6$ ,  $F11$ ). Results from all models and locations are available in Supporting Information Tables A3 -A5. Overall statistics indicate that HRRR and RDPS provide the best description of the wind structure of Hurricane Dorian.

Example maps of DUNEX-RT results for September 6 18:00 UTC from the 00Z run are shown with observations (Figure 4 b-d) for the HRRR forecasted wind input (Figure 4 a). At this time, waves are directed from north to south, with  $Hs = 5-6$  m on the shelf and  $Hs = 1-2$  m in the APES, and model results generally agree with observations (Figure 4 b). The strong northern winds drove water toward the southern shores of the APES and produced up to 1.5 m of surge in the large back-barrier estuary (Figure 4 c). A strong (1.5 m/s) southward alongshore current on the shelf, driven primarily by wind, occurred offshore of the Outer Banks, and is in agreement with the observations at  $F6$  and  $F11$  (Figure 4 d), with measured and predicted currents of up to 0.9 m/s in Currituck Sound.

The model results for different wind forecast inputs are shown through time with observations in Figure 5. Earlier forecasts are shown in green, with later forecast in blue, which illustrates the impacts of differences in atmospheric forcing and helps identify areas with higher or lower errors. Water levels forecasts are accurate and relatively consistent, particularly near inlets, with a RMSD of 0.13 m at Oregon Inlet ( $OI$ , Figure 5 c). Wave heights are subject to additional variation with changes in response to boundary forecasts and winds; however, overall results were fairly accurate, with a RMSD of 0.77 m at an offshore wave

buoy with a peak observed  $H_s$  of 4.5 m (*F17*, Figure 5 f). Current velocity observations on the inner shelf are very strong (1-2 m/s) during the hurricane and thus closely depend on the input wind field, demonstrated by the very different model predictions at *F6* and *F11* through time (Figure 5 h-i). A more accurate wind field occurred in earlier HRRR forecasts, and this is communicated through the overlapping curves that terminate in a vertical line at the end of each forecast period. Despite this, depth-averaged velocity RMSDs remained low, with errors of 0.18 m/s and 0.20 m/s at FRF sites *F6* and *F11*. Displaying these changing results in real-time intuitively communicates differences between model results, forecast runs, and observations, without the additional pre-event computational demands of a probabilistic model (e.g. Irish et al. 2011). For the case of Hurricane Dorian, the statistics that quantify agreement (RMSD and R) between model results and observations at all sites are quantified in Supporting Information Tables A3-A5.

## 4 Conclusions

Although existing modelling systems can provide coastal forecasts, limitations in resolution, real-time validation, and interactive output results constrain their use for rapid research applications. To address these challenges, a high-resolution real-time model called DUNEX-RT was developed using Delft3D-SWAN and was implemented for the Outer Banks region of NC, USA. This paper describes the performance of the modelling system during the September 2019 crossing of Hurricane Dorian. After evaluating 7 atmospheric hindcasts, the Regional Deterministic Prediction System (RDPS) and the High Resolution Rapid Refresh model (HRRR) were selected for evaluation in a forecast configuration. Effective coastal forecasts were obtained from both atmospheric forecast models, with lower errors from the HRRR model for water levels and waves. Overall, depth-averaged velocity forecasts were more accurate when using the RDPS model.

Relying on accurately forecasted inputs from larger scale atmospheric, ocean, and wave models as boundary conditions, the DUNEX-RT system provides high-resolution regional results with modest computational resources. The application of accurate boundary condition forecasts from multiple large-scale models represents a method of optimizing computational resources to advance accurate forecasts of coastal conditions. This produces useful predictions to assist in instrumentation deployment prior to storm events that is communicated through an interactive web interface. The presentation of varying model outputs through time together with observations intuitively conveys the impact of wind model accuracy and

256 uncertainty in real-time. Research should continue to investigate differences in wind field  
257 models during future storms and evaluate the impact of 2D vs 3D models for simulating  
258 coastal processes. Future work could also include analysis of results over a longer time  
259 period to characterize accuracy of these atmospheric forecasts. The results presented here  
260 suggest that this novel method of developing a high-resolution regional modelling system  
261 can also be accurately applied to forecast conditions in other areas of the coastal ocean.

## Acknowledgments

The authors thank the USCRP and the DUNEX community, including Britt Raubenheimer at the Woods Hole Oceanographic Institution, Spicer Bak and Ian Conery at the USACE Field Research Facility, D. Reide Corbett at the East Carolina University Coastal Studies Institute (CSI), and Allison Penko at the U.S. Naval Research Laboratory (NRL). Research funding for this project was provided by the US Office of Naval Research (ONR) Global science program with a Naval International Cooperative Opportunities in Science and Technology (NICOP) grant awarded to R. Mulligan under award number N62909-17-1-2169, and the Queen's University Engineering Dean's Graduate Research Award held by A. Rey. R. P. Mulligan also acknowledges support from the Natural Science and Engineering Research Council of Canada Discovery Grant Program under award number RGPIN/04043-2018. Computational support was provided by SHARCNET ([www.sharcnet.ca](http://www.sharcnet.ca)), Compute Canada (<http://computeCanada.ca>), Cory Wyatt at Queen's University, and Maria Aristizabal Vargas at Rutgers University. The data used in this study are archived in the Department of Civil Engineering at Queen's University and are available will be made available in a data repository that is accessible prior to publication (doi: to be assigned). The DUNEX-RT model results are available at <http://coastlines.engineering.queensu.ca/dunexrt>.



Table 1: Summary of large-scale model outputs used as input to DUNEX-RT

Type	Atmospheric Hindcasts				
Abbreviation	GFS	NAM	CFSv2	RAP	ERA5
Name	Global Forecast System	North American Mesoscale Forecast System	Climate Forecast System v2	Rapid Refresh	European Reanalysis
Reference	Yang et al. (2006)	Rogers et al. (2009)	Saha et al. (2010)	Benjamin et al. (2016)	Hersbach and Dee (2016)
Source	NOAA	NOAA	NOAA	NOAA	ECMWF
Domain	Global	North America	Global	CONUS	Global
Horizontal res.	27 km	12 km	27 km	13 km	30 km
Output time step	6 h	6 h	1 h	1 h	1 h
Type	Atmospheric Forecasts		Ocean Boundary Forecasts		
Abbreviation	RDPS	HRRR	ESTOFS	NCOM	NWW3
Name	Regional Deterministic Prediction System	High Resolution Rapid Refresh	Extratropical Surge and Tide Operational Forecast System	Navy Coastal Ocean Model	Multigrid WaveWatch III
Reference	Caron et al. (2015)	Smith et al. (2008)	Funakoshi et al. (2012)	Martin et al. (2009)	Chawla et al. (2013)
Source	Env. Can.	NOAA	NOAA	NAVOCEANO	NOAA
Domain	North America	CONUS	North Atlantic	Global	Global
Horizontal res.	2.5 km	3.5 km	0.2 km	3.7 km	6.7 km
Output time step	1 h	1 h	1 h	3 h	3 h

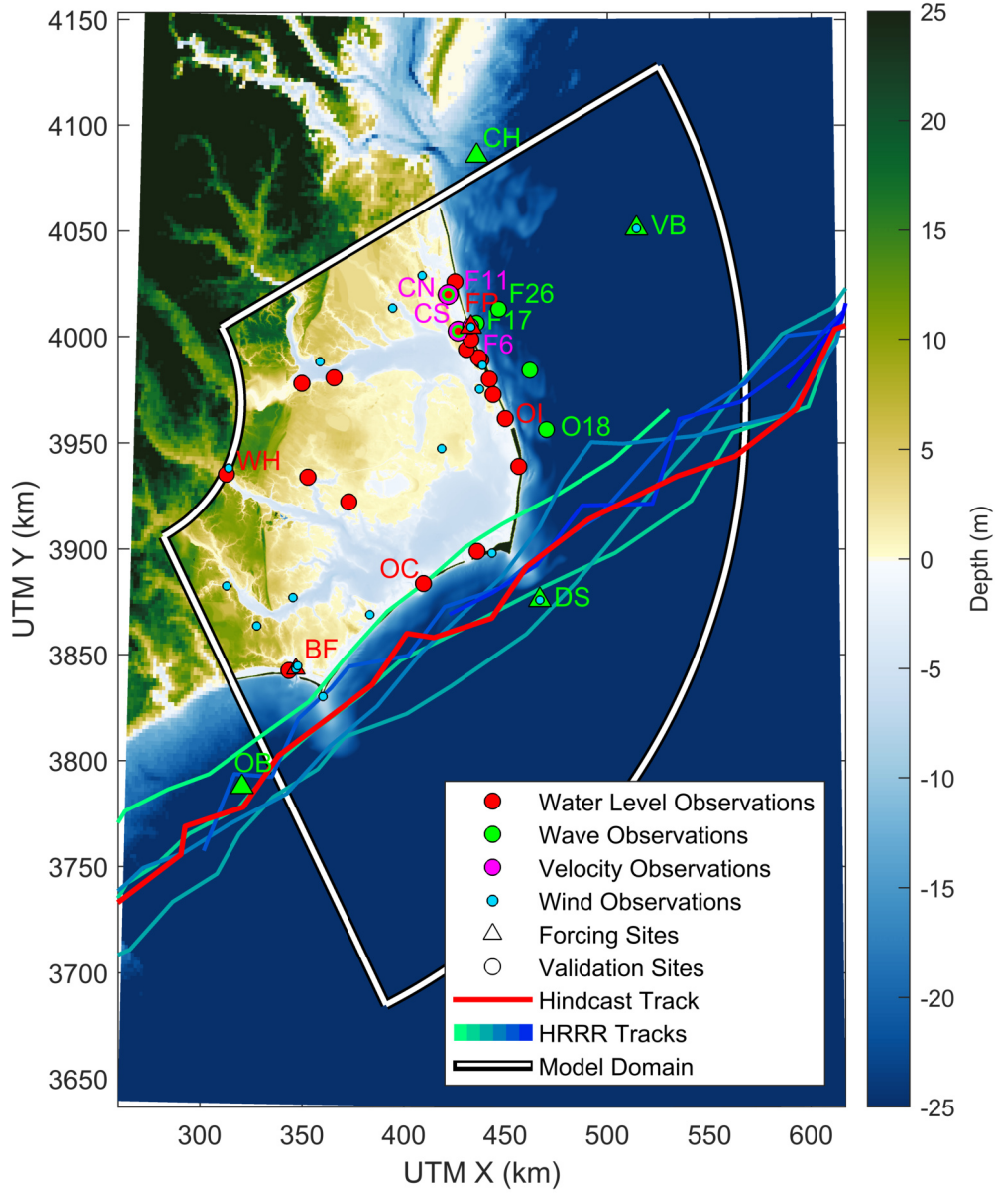


Figure 1: Map of the DUNEX-RT model domain including bathymetry, model boundaries, selected validation sites, and High Resolution Rapid Refresh (HRRR) forecast tracks for Hurricane Dorian every 6 hours. A map with all sites labelled is shown in Supporting Information Figure A1.

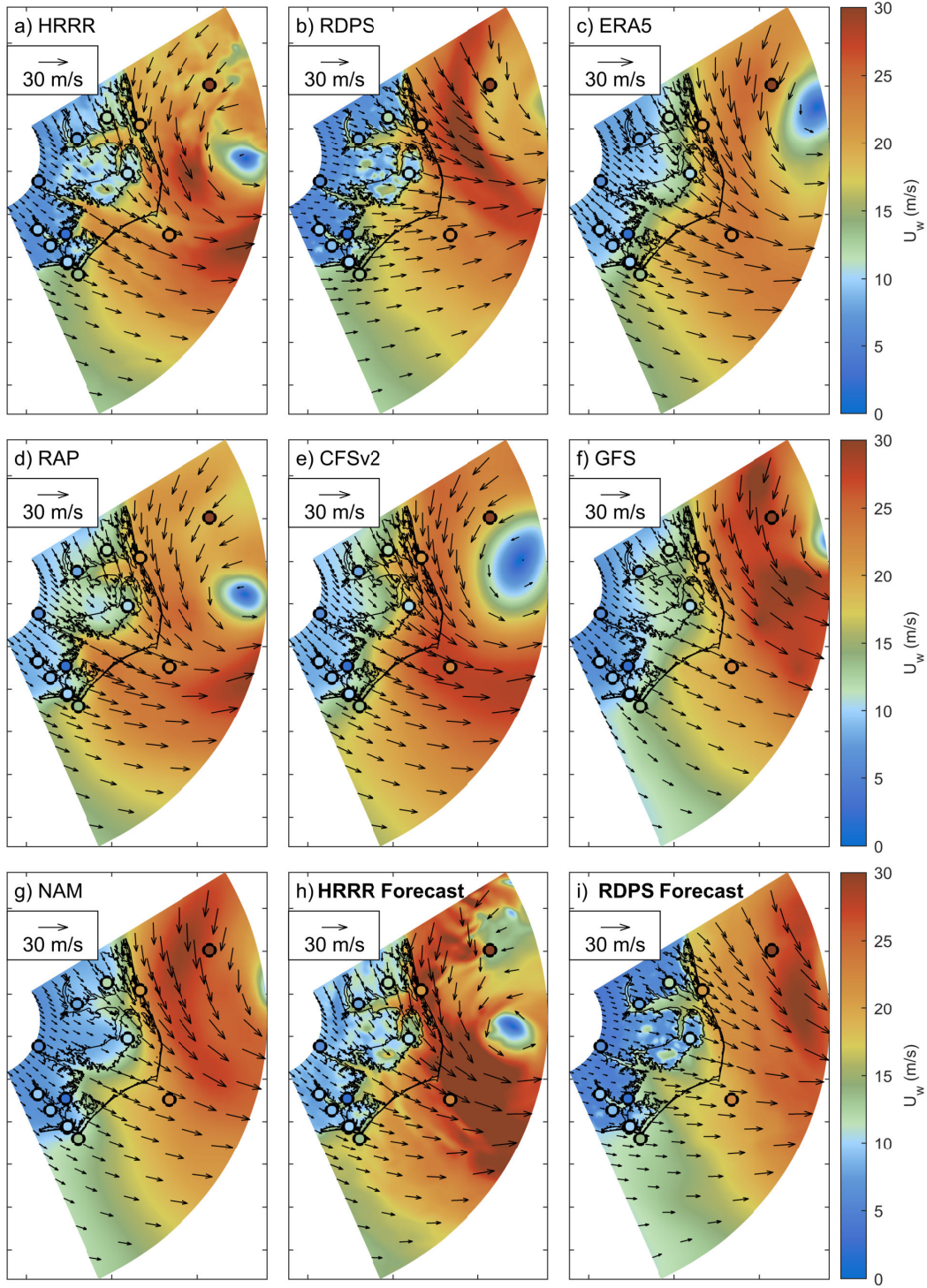


Figure 2: Comparison of hindcast and forecast ind fields on September 6 at 18:00 UTC: a) - g) 7 wind model hindcasts; h) - i) 2 wind model 18-hour (18Z) forecast products from simulations started on September 6 at 00:00 UTC. Observations are shown by coloured circles on the same scale.

–16–

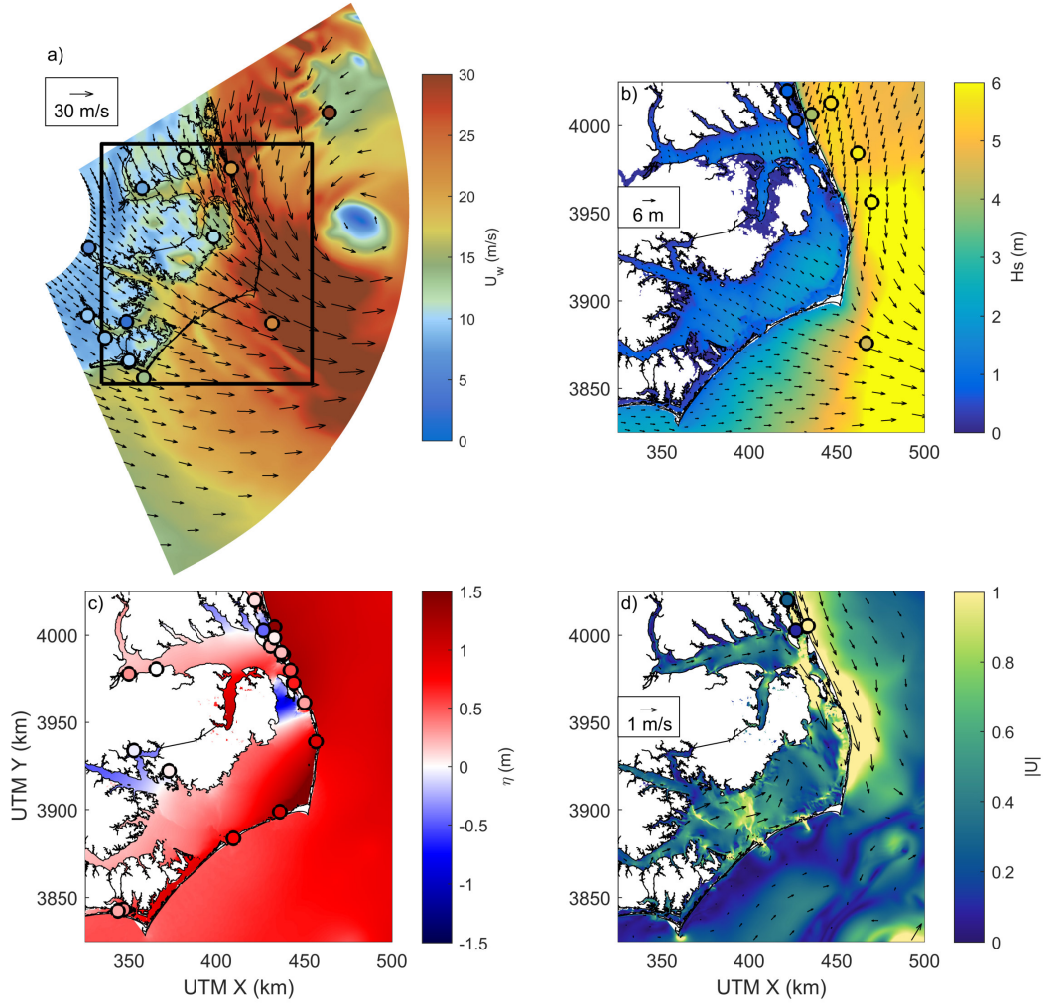


Figure 4: Example maps of model forcing and results on September 6, 2019 at 18:00 UTC: a) winds forecasted from the September 6 00:00 UTC HRRR model run, with a black box indicating zoom area for subsequent plots; b) significant wave height; c) water levels; and d) depth-averaged currents. Observations are shown by coloured circles and model results are shown by the colour contours on the same scale. Additional times are shown in Supporting Information Figures A6 - A11.



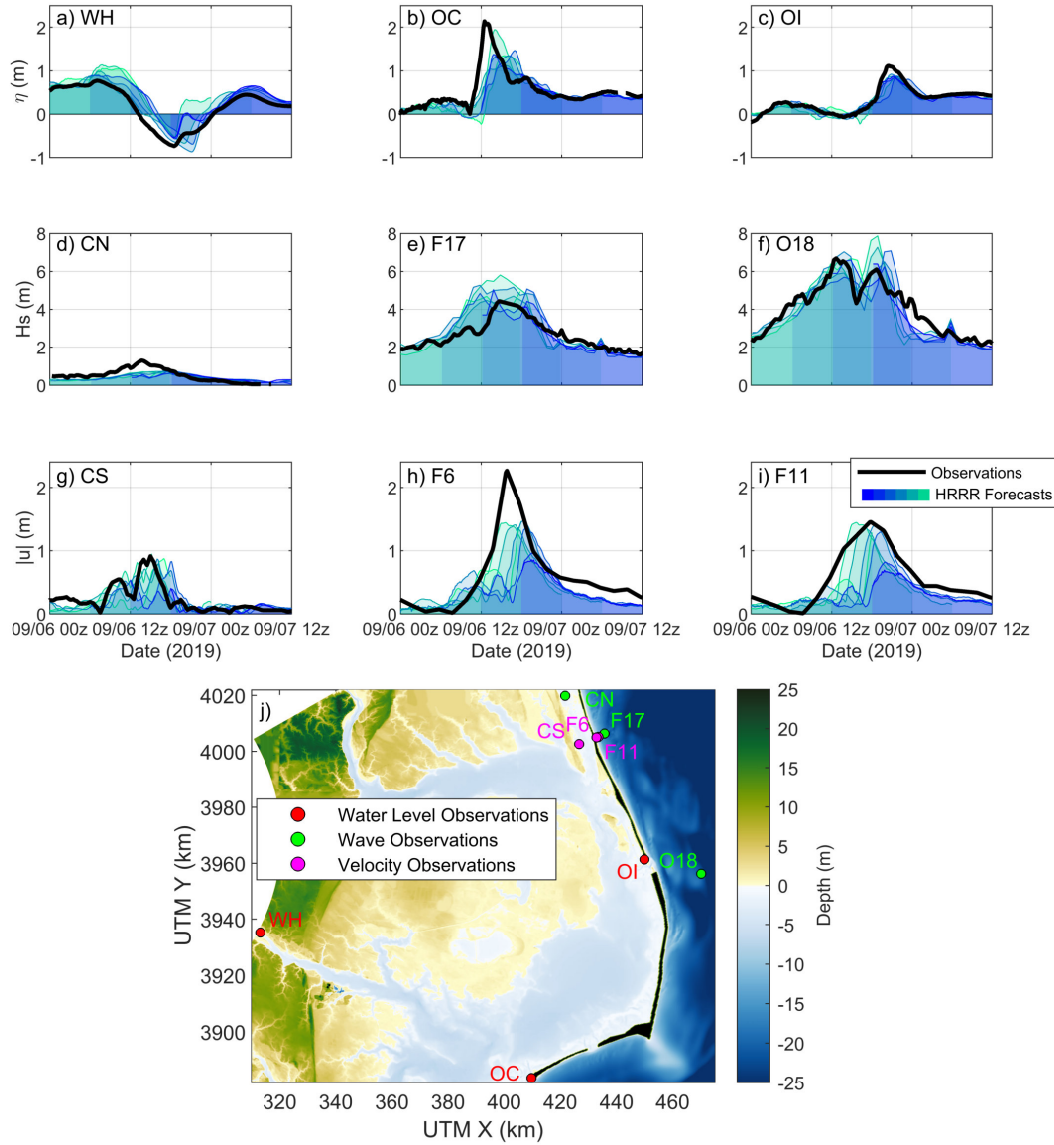


Figure 5: Observations (black line) and six different 36-hour HRRR forecast time-series results at selected sites across the system: a) - c) water levels; d) - f) significant wave height; g) - i) depth-averaged currents; and j) bathymetry and selected sites. Observations and model results for all sites are shown in Supporting Information Figures A3 - A5.

## References

- Agrawal, S., Barrington, L., Bromberg, C., Burge, J., Gazen, C., Hickey, J., 2019. Machine Learning for Precipitation Nowcasting from Radar Images, in: 33rd Conference on Neural Information Processing Systems (NeurIPS 2019), Vancouver. pp. 1–6.   
**arXiv:1912.12132.**
- Aretxabaleta, A.L., Doran, K.S., Long, J.W., Erikson, L.H., Storlazzi, C.D., 2019. Toward a National Coastal Hazard Forecast of Total Water Levels, in: Rosati, J.D., Wang, P., Vallee, M. (Eds.), *Coastal Sediments 2019*, WORLD SCIENTIFIC, St. Petersburg, Florida. pp. 1373–1384. doi:10.1142/9789811204487\_0120.
- Benjamin, S.G., Weygandt, S.S., Brown, J.M., Hu, M., Alexander, C.R., Smirnova, T.G., Olson, J.B., James, E.P., Dowell, D.C., Grell, G.A., Lin, H., Peckham, S.E., Smith, T.L., Moninger, W.R., Kenyon, J.S., Manikin, G.S., 2016. A North American hourly assimilation and model forecast cycle: The rapid refresh. *Monthly Weather Review* 144, 1669–1694. doi:10.1175/MWR-D-15-0242.1.
- Bennett, V.C., Mulligan, R.P., 2017. Evaluation of surface wind fields for prediction of directional ocean wave spectra during Hurricane Sandy. *Coastal Engineering* 125, 1–15. doi:10.1016/j.coastaleng.2017.04.003.
- Bennett, V.C., Mulligan, R.P., Hapke, C.J., 2018. A numerical model investigation of the impacts of Hurricane Sandy on water level variability in Great South Bay, New York. *Continental Shelf Research* 161, 1–11. doi:10.1016/j.csr.2018.04.003.
- Beven, J., 2019. Hurricane Dorian Advisory Number 59. URL:   
<https://www.nhc.noaa.gov/archive/2019/al05/al052019.public.059.shtml?>
- Bilskie, M.V., Hagen, S.C., Medeiros, S.C., 2019. Unstructured finite element mesh decimation for real-time Hurricane storm surge forecasting. *Coastal Engineering* 156, 103622. doi:10.1016/j.coastaleng.2019.103622.
- Blanton, B., McGee, J., Fleming, J., Kaiser, C., Kaiser, H., Lander, H., Luettich, R., Dresback, K., Kolar, R., 2012. Urgent computing of storm surge for North Carolina’s coast. *Procedia Computer Science* 9, 1677–1686. doi:10.1016/j.procs.2012.04.185.
- Blaylock, B.K., Horel, J.D., Liston, S.T., 2017. Cloud archiving and data mining of High-Resolution Rapid Refresh forecast model output. *Computers and Geosciences* 109, 43–50. doi:10.1016/j.cageo.2017.08.005.
- Booij, N., Ris, R.C., Holthuijsen, L.H., 1999. A third-generation wave model for coastal regions 1. Model description and validation. *Journal of Geophysical Research: Oceans*

- 104, 7649–7666. doi:10.1029/98JC02622.
- Cangialosi, J., 2019. Hurricane Dorian Advisory Number 52. URL:  
<https://www.nhc.noaa.gov/archive/2019/a105/a1052019.public.052.shtml?>
- Caron, J.F., Milewski, T., Buehner, M., Fillion, L., Reszka, M., Macpherson, S., St-James, J., 2015. Implementation of deterministic weather forecasting systems based on ensemble-variational data assimilation at Environment Canada. Part II: The regional system. *Monthly Weather Review* 143, 2560–2580. doi:10.1175/MWR-D-14-00353.1.
- Chawla, A., Tolman, H.L., Gerald, V., Spindler, D., Spindler, T., Alves, J.H.G., Cao, D., Hanson, J.L., Devaliere, E.M., 2013. A multigrid wave forecasting model: A new paradigm in operational wave forecasting. *Weather and Forecasting* 28, 1057–1078. doi:10.1175/WAF-D-12-00007.1.
- Cialone, M., Elko, N., Lillycrop, J., Stockdon, H., Raubenheimer, B., Rosati, J., 2019. During Nearshore Event Experiment (DUNEX): A Collaborative Community Field Data Collection Effort, in: Rosati, J.D., Wang, P., Vallee, M. (Eds.), *Coastal Sediments 2019*, WORLD SCIENTIFIC, St. Petersburg, Florida. pp. 2958–2966. doi:10.1142/9789811204487\_0253.
- Clunies, G.J., Mulligan, R.P., Mallinson, D.J., Walsh, J.P., 2017. Modeling hydrodynamics of large lagoons : Insights from the Albemarle-Pamlico Estuarine System. *Estuarine, Coastal and Shelf Science* 189, 90–103. doi:10.1016/j.ecss.2017.03.012.
- Copernicus Climate Change Service (C3S), 2017. ERA5: Fifth generation of ECMWF atmospheric reanalyses of the global climate. URL:  
<https://cds.climate.copernicus.eu>.
- Cyriac, R., Dietrich, J.C., Fleming, J.G., Blanton, B.O., Kaiser, C., Dawson, C.N., Luettich, R.A., 2018. Variability in Coastal Flooding predictions due to forecast errors during Hurricane Arthur. *Coastal Engineering* 137, 59–78. doi:10.1016/j.coastaleng.2018.02.008.
- Dietrich, J.C., Muhammad, A., Curcic, M., Fathi, A., Dawson, C.N., Chen, S.S., Luettich, R.A., 2018. Sensitivity of storm surge predictions to atmospheric forcing during Hurricane Isaac. *Journal of Waterway, Port, Coastal and Ocean Engineering* 144, 1–24. doi:10.1061/(ASCE)WW.1943-5460.0000419.
- Dresback, K.M., Fleming, J.G., Blanton, B.O., Kaiser, C., Gourley, J.J., Tromble, E.M., Luettich, R.A., Kolar, R.L., Hong, Y., Van Cooten, S., Vergara, H.J., Flamig, Z.L., Lander, H.M., Kelleher, K.E., Nemunaitis-Monroe, K.L., 2013. Skill assessment of a



- 345 real-time forecast system utilizing a coupled hydrologic and coastal hydrodynamic  
346 model during Hurricane Irene (2011). *Continental Shelf Research* 71, 78–94.  
347 doi:10.1016/j.csr.2013.10.007.
- 348 Drost, E.J., Lowe, R.J., Ivey, G.N., Jones, N.L., Péquignot, C.A., 2017. The effects of  
349 tropical cyclone characteristics on the surface wave fields in Australia’s North West  
350 region. *Continental Shelf Research* 139, 35–53. doi:10.1016/j.csr.2017.03.006.
- 351 Edwards, K., Nguyen, T., Sitton, D., 2012. Generating Delft3D Boundary Conditions  
352 Using the Navy Coastal Ocean Model. Technical Report. Naval Research Laboratory.  
353 Stennis Space Center, MS.
- 354 Elko, N., Dietrich, J., Cialone, M., Stockdon, H., Bilskie, M., Boyd, B., Charbonneau, B.,  
355 Cox, D., Dresback, K., Elgar, S., Lewis, A., Limber, P., Long, J., Massey, T., Mayo, T.,  
356 McIntosh, K., Nadal-Caraballo, N., Raubenheimer, B., Tomiczek, T., Wargula, A., 2019.  
357 Advancing the understanding of storm processes and impacts. *Shore and Beach* 87,  
358 41–55.
- 359 Elko, N., Feddersen, F., Foster, D., Hapke, C., Mcninch, J., Mulligan, R.P., 2015. The  
360 future of nearshore processes research. *Shore and Beach* 83, 13–38.
- 361 Elvidge, S., Angling, M.J., Nava, B., 2014. On the use of modified Taylor diagrams to  
362 compare ionospheric assimilation models, in: 2014 XXXIth URSI General Assembly and  
363 Scientific Symposium (URSI GASS), IEEE. pp. 1–4.  
364 doi:10.1109/URSIGASS.2014.6929835.
- 365 FEMA, 2019. Preliminary Damage Assessment Report: North Carolina - Hurricane  
366 Dorian. Technical Report. Federal Emergency Management Agency. URL:  
367 <https://www.fema.gov/media-library/assets/documents/184451>.
- 368 Ferreira, C., 2017. iFLOOD: A Real Time Flood Forecast System for Total Water  
369 Modeling in the National Capital Region, in: AGU Fall Meeting Abstracts, New  
370 Orleans, Louisiana. pp. NH41A–0153.
- 371 Flick, R.E., McGehee, D.D., Seymour, R.J., Guza, R.T., 1993. The Coastal Data  
372 Information Program—A Successful Federal, State and University Cooperation, in:  
373 Coastal Engineering Considerations in Coastal Zone Management, ASCE. pp. 245–249.
- 374 Funakoshi, Y., Feyen, J., Aikman, F., Tolman, H., van der Westhuysen, A., Chawla, A.,  
375 Rivin, I., Taylor, A., 2012. Development of Extratropical Surge and Tide Operational  
376 Forecast System (ESTOFS), in: Estuarine and Coastal Modeling, American Society of  
377 Civil Engineers, Reston, VA. pp. 201–212. doi:10.1061/9780784412411.00012.

- 378 Garzon, J.L., Ferreira, C.M., Padilla-Hernandez, R., 2018. Evaluation of weather forecast  
379 systems for storm surge modeling in the Chesapeake Bay. *Ocean Dynamics* 68, 91–107.  
380 doi:10.1007/s10236-017-1120-x.
- 381 Gittman, R.K., Popowich, A.M., Bruno, J.F., Peterson, C.H., 2014. Marshes with and  
382 without sills protect estuarine shorelines from erosion better than bulkheads during a  
383 Category 1 hurricane. *Ocean and Coastal Management* 102, 94–102.  
384 doi:10.1016/j.ocecoaman.2014.09.016.
- 385 Grinsted, A., Ditlevsen, P., Christensen, J.H., 2019. Normalized US hurricane damage  
386 estimates using area of total destruction 1900-2018. *Proceedings of the National*  
387 *Academy of Sciences* 116, 23942–23946. doi:10.1073/pnas.1912277116.
- 388 Hersbach, H., Dee, D., 2016. ERA5 reanalysis is in production, *ECMWF Newsletter* 147,  
389 *ECMWF. ECMWF Newsletter Vol. 147, 7.*
- 390 Herzmann, D., Arritt, R., Todey, D., 2004. Iowa environmental mesonet. Available at  
391 mesonet. agron. iastate. edu/request/coop/fe. phtml (verified 27 Sept. 2005). Iowa State  
392 Univ., Dep. of Agron., Ames, IA .
- 393 Irish, J.L., Song, Y.K., Chang, K.A., 2011. Probabilistic hurricane surge forecasting using  
394 parameterized surge response functions. *Geophysical Research Letters* 38, 1–5.  
395 doi:10.1029/2010GL046347.
- 396 Knutson, T.R., McBride, J.L., Chan, J., Emanuel, K., Holland, G., Landsea, C., Held, I.,  
397 Kossin, J.P., Srivastava, A.K., Sugi, M., 2010. Tropical cyclones and climate change.  
398 *Nature Geoscience* 3, 157–163. doi:10.1038/ngeo779.
- 399 Lesser, G.R., Roelvink, J.A., van Kester, J.A., Stelling, G.S., 2004. Development and  
400 validation of a three-dimensional morphological model. *Coastal Engineering* 51,  
401 883–915. doi:10.1016/j.coastaleng.2004.07.014.
- 402 Lixion, A., Cangialosi, J., 2019. Hurricane Dorian Advisory Number 34. URL:  
403 <https://www.nhc.noaa.gov/archive/2019/a105/a1052019.public.034.shtml?>
- 404 Mai, J., Kornelsen, K.C., Tolson, B.A., Fortin, V., Gasset, N., Bouhemhem, D., Schäfer,  
405 D., Leahy, M., Anctil, F., Coulibaly, P., 2019. The Canadian Surface Prediction Archive  
406 (CaSPAR): A Platform to Enhance Environmental Modeling in Canada and Globally.  
407 *Bulletin of the American Meteorological Society* doi:10.1175/bams-d-19-0143.1.
- 408 Martin, P.J., Barron, C.N., Smedstad, L.F., Campbell, T.J., Wallcraft, A.J., Rhodes, R.C.,  
409 Rowley, C., Townsend, T.L., Carroll, S.N., 2009. User’s Manual for the Navy Coastal  
410 Ocean Model (NCOM) Version 4.0. Technical Report. Naval Research Lab Stennis

- 411 Space Center Ms Ocean Dynamics and Prediction Branch. URL:  
412 <https://apps.dtic.mil/docs/citations/ADA508063>.
- 413 Mulligan, R.P., Hanson, J.L., 2016. Alongshore momentum transfer to the nearshore zone  
414 from energetic ocean waves generated by passing hurricanes. *Journal of Geophysical*  
415 *Research: Oceans* 121, 4178–4193. doi:10.1002/2016JC011706.
- 416 Mulligan, R.P., Hay, A.E., Bowen, A.J., 2008. Wave-driven circulation in a coastal bay  
417 during the landfall of a hurricane. *Journal of Geophysical Research: Oceans* 113, 1–10.  
418 doi:10.1029/2007JC004500.
- 419 Mulligan, R.P., Mallinson, D.J., Clunies, G.J., Rey, A., Culver, S.J., Zaremba, N., Leorri,  
420 E., Mitra, S., 2019. Estuarine Responses to Long-Term Changes in Inlets, Morphology,  
421 and Sea Level Rise. *Journal of Geophysical Research: Oceans* 124, 9235–9257.  
422 doi:10.1029/2018JC014732.
- 423 Mulligan, R.P., Perrie, W., Toulany, B., Smith, P.C., Hay, A.E., Bowen, A.J., 2011.  
424 Performance of nowcast and forecast wave models for Lunenburg Bay, Nova Scotia.  
425 *Atmosphere - Ocean* 49, 1–7. doi:10.1080/07055900.2011.558468.
- 426 Mulligan, R.P., Walsh, J.P., Wadman, H.M., 2015. Storm Surge and Surface Waves in a  
427 Shallow Lagoonal Estuary during the Crossing of a Hurricane. *Journal of Waterway,*  
428 *Port, Coastal, and Ocean Engineering* 141, 1–11.  
429 doi:10.1061/(ASCE)WW.1943-5460.0000260.
- 430 National Weather Service, 2019. Post Tropical Cyclone Report: Hurricane Dorian.  
431 Technical Report. National Weather Service. Raleigh, NC. URL:  
432 <https://www.weather.gov/media/rah/HurricaneDorian/DorianPSH.pdf>.
- 433 NOAA National Centers for Environmental Information, 2016. U.S. Coastal Relief Model.  
434 URL: <http://www.ngdc.noaa.gov/mgg/coastal/crm.html>, doi:10.7289/V53R0QR5.
- 435 Olabarrieta, M., Warner, J.C., Kumar, N., 2011. Wave-current interaction in Willapa Bay.  
436 *Journal of Geophysical Research: Oceans* 116, 1–27. doi:10.1029/2011JC007387.
- 437 Paramygin, V., Sheng, Y., Davis, J., 2017. Towards the Development of an Operational  
438 Forecast System for the Florida Coast. *Journal of Marine Science and Engineering* 5, 8.  
439 doi:10.3390/jmse5010008.
- 440 Powell, M.D., Murillo, S., Dodge, P., Uhlhorn, E., Gamache, J., Cardone, V., Cox, A.,  
441 Otero, S., Carrasco, N., Annane, B., Fleur, R.S., 2010. Reconstruction of Hurricane  
442 Katrina’s wind fields for storm surge and wave hindcasting. *Ocean Engineering* 37,  
443 26–36. doi:10.1016/j.oceaneng.2009.08.014.

- 444 Rogers, E., DiMego, G., Black, T., Ek, M., Ferrier, B., Gayno, G., Janjic, Z., Lin, Y., Pyle,  
445 M., Wong, V., 2009. The NCEP North American mesoscale modeling system: Recent  
446 changes and future plans, in: Preprints, 23rd Conference on Weather Analysis and  
447 Forecasting/19th Conference on Numerical Weather Prediction.
- 448 Royal Meteorological Society, 2019. Weather news. *Weather* 74, 330–331.  
449 doi:10.1002/wea.3352.
- 450 Saha, S., Moorthi, S., Pan, H.L., Wu, X., Wang, J., Nadiga, S., Tripp, P., Kistler, R.,  
451 Woollen, J., Behringer, D., Liu, H., Stokes, D., Grumbine, R., Gayno, G., Wang, J.,  
452 Hou, Y.T., Chuang, H.y., Juang, H.M.H., Sela, J., Iredell, M., Treadon, R., Kleist, D.,  
453 Van Delst, P., Keyser, D., Derber, J., Ek, M., Meng, J., Wei, H., Yang, R., Lord, S.,  
454 van den Dool, H., Kumar, A., Wang, W., Long, C., Chelliah, M., Xue, Y., Huang, B.,  
455 Schemm, J.K., Ebisuzaki, W., Lin, R., Xie, P., Chen, M., Zhou, S., Higgins, W., Zou,  
456 C.Z., Liu, Q., Chen, Y., Han, Y., Cucurull, L., Reynolds, R.W., Rutledge, G., Goldberg,  
457 M., 2010. The NCEP Climate Forecast System Reanalysis. *Bulletin of the American*  
458 *Meteorological Society* 91, 1015–1058. doi:10.1175/2010BAMS3001.1.
- 459 Sheng, Y.P., Alymov, V., Paramygin, V.A., 2010. Simulation of storm surge, wave,  
460 currents, and inundation in the outer banks and Chesapeake bay during Hurricane  
461 Isabel in 2003: The importance of waves. *Journal of Geophysical Research: Oceans* 115.  
462 doi:10.1029/2009JC005402.
- 463 Smith, T.L., Benjamin, S.G., Brown, J.M., Weygandt, S., Smirnova, T., Schwartz, B.,  
464 2008. Convection forecasts from the hourly updated, 3-km High Resolution Rapid  
465 Refresh (HRRR) model. URL:  
466 [https://ams.confex.com/ams/24SLS/techprogram/paper/{\\_}142055.htm](https://ams.confex.com/ams/24SLS/techprogram/paper/{_}142055.htm).
- 467 Stelling, G.S., 1983. On the construction of computational methods for shallow water flow  
468 problems. Phd. TU Delft. Delft. URL:  
469 <http://resolver.tudelft.nl/uuid:d3b818cb-9f91-4369-a03e-d90c8c175a96>.
- 470 Taylor, K.E., 2001. Summarizing multiple aspects of model performance in a single  
471 diagram. *Journal of Geophysical Research: Atmospheres* 106, 7183–7192.  
472 doi:10.1029/2000JD900719.
- 473 Thomas, A., Dietrich, J.C., Asher, T.G., Bell, M., Blanton, B.O., Copeland, J.H., Cox,  
474 A.T., Dawson, C.N., Fleming, J.G., Luettich, R.A., 2019. Influence of storm timing and  
475 forward speed on tides and storm surge during Hurricane Matthew. *Ocean Modelling*  
476 137, 1–19. doi:10.1016/j.ocemod.2019.03.004.

- UNICEF, 2019. Hurricane Dorian The Bahamas Humanitarian Situation in Numbers  
Situation Overview & Humanitarian Needs. Technical Report 4. United Nations. URL:  
[https://reliefweb.int/report/bahamas/hurricane-dorian-bahamas](https://reliefweb.int/report/bahamas/hurricane-dorian-bahamas-humanitarian-situation-report-no-4-reporting-period-25)  
[-humanitarian-situation-report-no-4-reporting-period-25](https://reliefweb.int/report/bahamas/hurricane-dorian-bahamas-humanitarian-situation-report-no-4-reporting-period-25).
- Xie, X., Li, M., Ni, W., 2018. Roles of Wind-Driven Currents and Surface Waves in  
Sediment Resuspension and Transport During a Tropical Storm. *Journal of Geophysical*  
*Research: Oceans* 123, 8638–8654. doi:10.1029/2018JC014104.
- Yang, F., Pan, H.L., Krueger, S.K., Moorthi, S., Lord, S.J., 2006. Evaluation of the NCEP  
global forecast system at the ARM SGP site. *Monthly Weather Review* 134, 3668–3690.  
doi:10.1175/MWR3264.1.

## **Appendix A Supporting Information**

Table A1: List of Data Sources.

ID	Name	Parameters	Grid/ Depth	Source
FP	FRF Pier	Water Level; Wind	6 m	USACE
BF	Beaufort Duke Marine Lab	Water Level; Wind	N/A	NOAA/ Duke
VB	Virginia Beach Wave	Wave; Wind	47 m	NDBC/ USACE
DS	Diamond Shoals Buoy	Wave; Wind	59 m	NDBC
OB	Oslo Bay Buoy	Wave	30 m	CDIP/ USACE
CH	Cape Henry Buoy	Wave	18 m	CDIP/ USACE
CN	Currituck Sound North	Water Level; Wave; Current	2.3 m	UNC
CS	Currituck Sound South	Water Level; Wave; Current	2.6 m	UNC
F11	FRF AWAC	Current	11 m	USACE
NH	Nags Head Buoy	Wave	21 m	NDBC/ UNC
O18	Oregon Inlet Buoy	Wave	18 m	NDBC/ UNC
F17	FRF 17 m Buoy	Wave	17 m	USACE
F26	FRF 26 m Buoy	Wave	26 m	USACE
OC	Coast Guard Station @ Ocracoke	Water Level; Wind	N/A	ISU/ HADS
OI	Oregon Inlet Marina	Water Level	N/A	NOAA
AB	Bogue Sound @ Atlantic Beach	Water Level	N/A	USGS
HT	Hatteras Coast Guard	Water Level	N/A	NOAA/ USCG
AS	Albemarle Sound @ Leonards Point	Water Level	N/A	USGS
CC	Currituck Sound @ Corolla	Water Level	N/A	USGS
PH	Currituck Sound @ Point Harbour	Water Level	N/A	USGS
JC	Jean Guite Creek Outlet	Water Level	N/A	USACE
HD	Kill Devil Hills @ Hayman Street	Water Level	N/A	USACE
VD	Villa Dunes Dock	Water Level	N/A	USACE
PI	Roanoke Sound @ Point Island	Water Level	N/A	USGS
KH	Albemarle Sound @ Kitty Hawk	Water Level	N/A	ISU/ HADS
WO	Roanoke River @ Westover	Water Level	N/A	ISU/ HADS
BH	Pungo River @ Belhaven	Water Level	N/A	ISU/ HADS
WH	Pamlico River @ Washington	Water Level	N/A	ISU/ HADS
BI	Pamlico Sound @ Bell Island Pier	Water Level	N/A	ISU/ HADS
RF	Pamlico Sound @ Rodanthe	Water Level	N/A	ISU/ HADS
	Ferry Terminal			

Table A2: List of Wind Data Sources.

ID	Name	Elevation (NAVD 88 m)	Source
FP	FRF Pier	11.40 m	USACE
BF	Beaufort Duke Marine Lab	0.00 m	NOAA/ Duke
VB	Virginia Beach Wave	0.00 m	NDBC/ USACE
DS	Diamond Shoals Buoy	0.00 m	NDBC
CPL	Cape Lookout	4.60 m	NDBC
EDE	Edenton Northeast Airport	6.10 m	NWS
ECG	Elizabeth City Coast Guard	7.50 m	NWS
CPM	Cherry Point Marine Corps Air Station	9.90 m	NWS
EWN	Coastal Carolina Airport	6.10 m	NWS
OCW	Warren Field Airport	11.80 m	NWS
NRO	Neuse River @ Oriental	1.40 m	ISU/ HADS
LOA	Lola	3.74 m	ISU/ HADS
DCG	Dare County Gunnery Range	0.51 m	ISU/ ASOS
FFA	First flight Airport	4.00 m	ISU/ ASOS
HTA	Hatteras Airport	3.00 m	ISU/ ASOS
MDA	Manteo Dare Airport	4.00 m	ISU/ ASOS
BFA	Beaufort Airport	3.00 m	ISU/ ASOS
CCA	Currituck Country Airport	5.50 m	ISU/ ASOS



Table A3: Root-Mean-Square-Difference (upper, bold) and correlation coefficient (lower) for all water level observation points.

RMSD/R $\eta(m)$	FP	OI	BF	AB	AS	CN	CC	CS	PH	JC	HD	VD	PI	OC	KH	RF	WO	BH	WH	BI	Mean
Forecast HRRR	<b>0.12</b> 0.94	<b>0.08</b> 0.97	<b>0.20</b> 0.88	<b>0.19</b> 0.88	<b>0.15</b> 0.86	<b>0.11</b> 0.70	<b>0.09</b> 0.26	<b>0.16</b> 0.63	<b>0.11</b> 0.75	<b>0.15</b> 0.07	<b>0.15</b> 0.58	<b>0.20</b> 0.42	<b>0.18</b> 0.86	<b>0.31</b> 0.72	<b>0.11</b> 0.91	<b>0.16</b> 0.95	<b>0.10</b> 0.94	<b>0.21</b> 0.82	<b>0.15</b> 0.96	<b>0.26</b> 0.50	<b>0.16</b> 0.73
Forecast RDPS	<b>0.11</b> 0.95	<b>0.25</b> 0.67	<b>0.23</b> 0.85	<b>0.27</b> 0.79	<b>0.17</b> 0.82	<b>0.10</b> 0.83	<b>0.09</b> 0.25	<b>0.13</b> 0.79	<b>0.10</b> 0.81	<b>0.20</b> 0.00	<b>0.28</b> 0.16	<b>0.28</b> 0.28	<b>0.11</b> 0.95	<b>0.22</b> 0.91	<b>0.19</b> 0.69	<b>0.48</b> 0.56	<b>0.29</b> 0.54	<b>0.20</b> 0.85	<b>0.31</b> 0.75	<b>0.22</b> 0.64	<b>0.21</b> 0.65
HRRR	<b>0.15</b> 0.91	<b>0.12</b> 0.92	<b>0.13</b> 0.97	<b>0.14</b> 0.98	<b>0.15</b> 0.89	<b>0.10</b> 0.73	<b>0.06</b> 0.21	<b>0.15</b> 0.71	<b>0.12</b> 0.72	<b>0.09</b> 0.48	<b>0.08</b> 0.79	<b>0.16</b> 0.56	<b>0.22</b> 0.76	<b>0.35</b> 0.63	<b>0.15</b> 0.84	<b>0.20</b> 0.92	<b>0.13</b> 0.91	<b>0.20</b> 0.87	<b>0.18</b> 0.92	<b>0.26</b> 0.47	<b>0.16</b> 0.76
RDPS	<b>0.20</b> 0.83	<b>0.25</b> 0.76	<b>0.17</b> 0.96	<b>0.18</b> 0.98	<b>0.14</b> 0.89	<b>0.09</b> 0.82	<b>0.09</b> 0.33	<b>0.13</b> 0.79	<b>0.11</b> 0.82	<b>0.23</b> 0.00	<b>0.36</b> 0.29	<b>0.35</b> 0.44	<b>0.10</b> 0.96	<b>0.21</b> 0.94	<b>0.24</b> 0.72	<b>0.42</b> 0.75	<b>0.30</b> 0.61	<b>0.17</b> 0.91	<b>0.13</b> 0.96	<b>0.26</b> 0.41	<b>0.21</b> 0.71
ERA5	<b>0.17</b> 0.88	<b>0.12</b> 0.92	<b>0.14</b> 0.97	<b>0.15</b> 0.98	<b>0.18</b> 0.94	<b>0.11</b> 0.68	<b>0.06</b> 0.32	<b>0.17</b> 0.74	<b>0.12</b> 0.73	<b>0.11</b> 0.26	<b>0.13</b> 0.71	<b>0.18</b> 0.58	<b>0.18</b> 0.86	<b>0.33</b> 0.68	<b>0.12</b> 0.88	<b>0.23</b> 0.89	<b>0.18</b> 0.90	<b>0.30</b> 0.59	<b>0.24</b> 0.85	<b>0.27</b> 0.36	<b>0.17</b> 0.74
RAP	<b>0.16</b> 0.90	<b>0.09</b> 0.95	<b>0.16</b> 0.95	<b>0.16</b> 0.96	<b>0.20</b> 0.77	<b>0.13</b> 0.48	<b>0.06</b> 0.47	<b>0.18</b> 0.53	<b>0.10</b> 0.86	<b>0.12</b> 0.21	<b>0.14</b> 0.76	<b>0.19</b> 0.55	<b>0.21</b> 0.77	<b>0.36</b> 0.59	<b>0.09</b> 0.94	<b>0.19</b> 0.94	<b>0.17</b> 0.87	<b>0.31</b> 0.56	<b>0.25</b> 0.83	<b>0.29</b> 0.27	<b>0.18</b> 0.71
CFSv2	<b>0.17</b> 0.89	<b>0.11</b> 0.96	<b>0.12</b> 0.97	<b>0.13</b> 0.98	<b>0.18</b> 0.83	<b>0.13</b> 0.47	<b>0.10</b> 0.00	<b>0.21</b> 0.22	<b>0.15</b> 0.36	<b>0.10</b> 0.13	<b>0.12</b> 0.78	<b>0.14</b> 0.68	<b>0.20</b> 0.87	<b>0.37</b> 0.55	<b>0.17</b> 0.73	<b>0.23</b> 0.91	<b>0.14</b> 0.94	<b>0.31</b> 0.56	<b>0.24</b> 0.84	<b>0.28</b> 0.32	<b>0.18</b> 0.65
GFS	<b>0.20</b> 0.84	<b>0.17</b> 0.84	<b>0.09</b> 0.99	<b>0.14</b> 0.98	<b>0.21</b> 0.83	<b>0.15</b> 0.20	<b>0.06</b> 0.48	<b>0.23</b> 0.00	<b>0.11</b> 0.73	<b>0.17</b> 0.00	<b>0.17</b> 0.49	<b>0.19</b> 0.40	<b>0.18</b> 0.89	<b>0.36</b> 0.66	<b>0.13</b> 0.85	<b>0.28</b> 0.88	<b>0.18</b> 0.96	<b>0.24</b> 0.91	<b>0.26</b> 0.90	<b>0.22</b> 0.71	<b>0.19</b> 0.68
NAM	<b>0.18</b> 0.87	<b>0.15</b> 0.88	<b>0.10</b> 0.99	<b>0.13</b> 0.98	<b>0.21</b> 0.88	<b>0.10</b> 0.68	<b>0.06</b> 0.41	<b>0.20</b> 0.37	<b>0.12</b> 0.74	<b>0.14</b> 0.00	<b>0.13</b> 0.57	<b>0.16</b> 0.47	<b>0.19</b> 0.91	<b>0.33</b> 0.80	<b>0.14</b> 0.87	<b>0.28</b> 0.88	<b>0.21</b> 0.93	<b>0.23</b> 0.92	<b>0.29</b> 0.79	<b>0.20</b> 0.83	<b>0.18</b> 0.74

Table A4: Root-Mean-Square-Difference (upper, bold) and correlation coefficient (lower) for all wave observation points.

RMSD/R $Hs(m)$	VB	F26	NH	O18	F17	CN	CS	Mean
Forecast HRRR	<b>0.65</b> 0.86	<b>0.72</b> 0.85	<b>0.67</b> 0.90	<b>0.71</b> 0.90	<b>0.74</b> 0.87	<b>0.25</b> 0.70	<b>0.20</b> 0.79	<b>0.56</b> 0.84
Forecast RDPS	<b>0.64</b> 0.86	<b>0.96</b> 0.66	<b>0.95</b> 0.69	<b>0.99</b> 0.70	<b>0.76</b> 0.54	<b>0.18</b> 0.94	<b>0.16</b> 0.88	<b>0.66</b> 0.75
HRRR	<b>0.36</b> 0.96	<b>0.65</b> 0.86	<b>0.53</b> 0.92	<b>0.56</b> 0.92	<b>0.44</b> 0.88	<b>0.23</b> 0.81	<b>0.20</b> 0.81	<b>0.42</b> 0.88
RDPS	<b>0.70</b> 0.84	<b>0.89</b> 0.72	<b>0.86</b> 0.76	<b>0.74</b> 0.84	<b>0.74</b> 0.64	<b>0.18</b> 0.96	<b>0.18</b> 0.86	<b>0.61</b> 0.80
ERA5	<b>0.64</b> 0.86	<b>0.89</b> 0.72	<b>0.95</b> 0.70	<b>0.79</b> 0.82	<b>0.66</b> 0.69	<b>0.24</b> 0.82	<b>0.23</b> 0.74	<b>0.63</b> 0.76
RAP	<b>0.53</b> 0.91	<b>0.80</b> 0.78	<b>0.68</b> 0.86	<b>0.46</b> 0.95	<b>0.60</b> 0.81	<b>0.26</b> 0.71	<b>0.23</b> 0.73	<b>0.51</b> 0.82
CFSv2	<b>0.87</b> 0.84	<b>0.94</b> 0.72	<b>1.02</b> 0.72	<b>0.79</b> 0.86	<b>0.75</b> 0.76	<b>0.27</b> 0.66	<b>0.22</b> 0.74	<b>0.69</b> 0.76
GFS	<b>0.83</b> 0.78	<b>1.13</b> 0.54	<b>1.14</b> 0.60	<b>0.95</b> 0.75	<b>0.88</b> 0.50	<b>0.28</b> 0.58	<b>0.26</b> 0.55	<b>0.78</b> 0.61
NAM	<b>0.74</b> 0.82	<b>0.80</b> 0.78	<b>0.88</b> 0.76	<b>0.84</b> 0.81	<b>0.59</b> 0.75	<b>0.24</b> 0.81	<b>0.24</b> 0.68	<b>0.62</b> 0.77

Table A5: Root-Mean-Square-Difference (upper, bold) and correlation coefficient (lower) for all depth averaged velocity observation points.

RMSD/R $U(m/s)$	F6	F11	CN	CS	Mean
Forecast HRRR	<b>0.42</b> 0.66	<b>0.25</b> 0.81	<b>0.14</b> 0.63	<b>0.17</b> 0.68	<b>0.25</b> 0.69
Forecast RDPS	<b>0.34</b> 0.87	<b>0.22</b> 0.88	<b>0.08</b> 0.88	<b>0.15</b> 0.76	<b>0.20</b> 0.85
HRRR	<b>0.40</b> 0.73	<b>0.24</b> 0.87	<b>0.14</b> 0.53	<b>0.14</b> 0.80	<b>0.23</b> 0.73
RDPS	<b>0.29</b> 0.92	<b>0.19</b> 0.89	<b>0.09</b> 0.84	<b>0.12</b> 0.85	<b>0.17</b> 0.88
ERA5	<b>0.51</b> 0.39	<b>0.32</b> 0.71	<b>0.13</b> 0.64	<b>0.18</b> 0.57	<b>0.28</b> 0.58
RAP	<b>0.47</b> 0.53	<b>0.34</b> 0.63	<b>0.15</b> 0.42	<b>0.19</b> 0.51	<b>0.29</b> 0.53
CFSv2	<b>0.52</b> 0.36	<b>0.31</b> 0.71	<b>0.19</b> 0.18	<b>0.18</b> 0.58	<b>0.30</b> 0.46
GFS	<b>0.58</b> 0.08	<b>0.37</b> 0.50	<b>0.17</b> 0.17	<b>0.21</b> 0.30	<b>0.33</b> 0.26
NAM	<b>0.43</b> 0.67	<b>0.33</b> 0.67	<b>0.13</b> 0.61	<b>0.16</b> 0.73	<b>0.26</b> 0.67

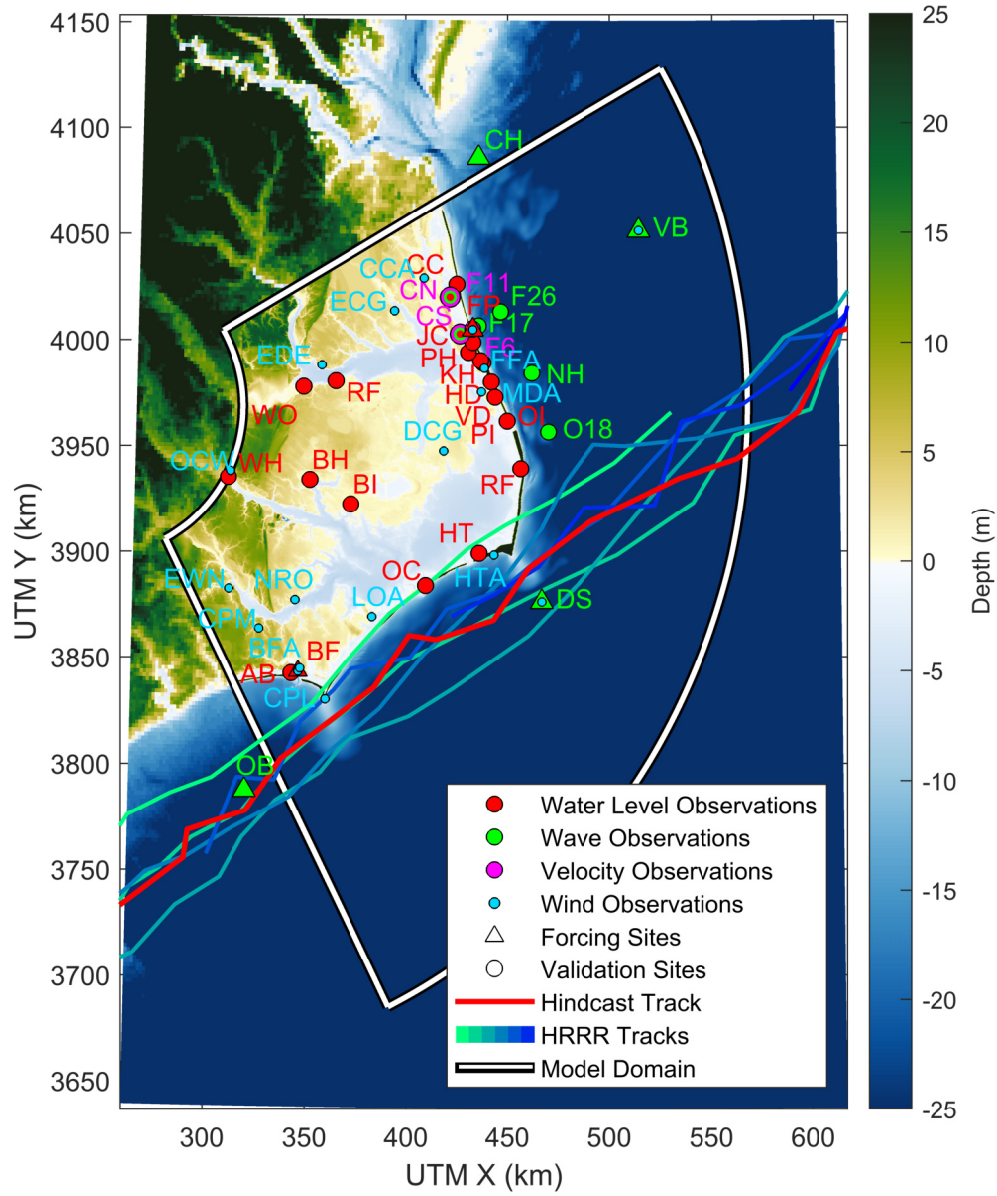


Figure A1: Map of the DUNEX-RT model domain including bathymetry, model boundaries, all validation sites, and High Resolution Rapid Refresh (HRRR) forecast tracks for Hurricane Dorian every 6 hours.

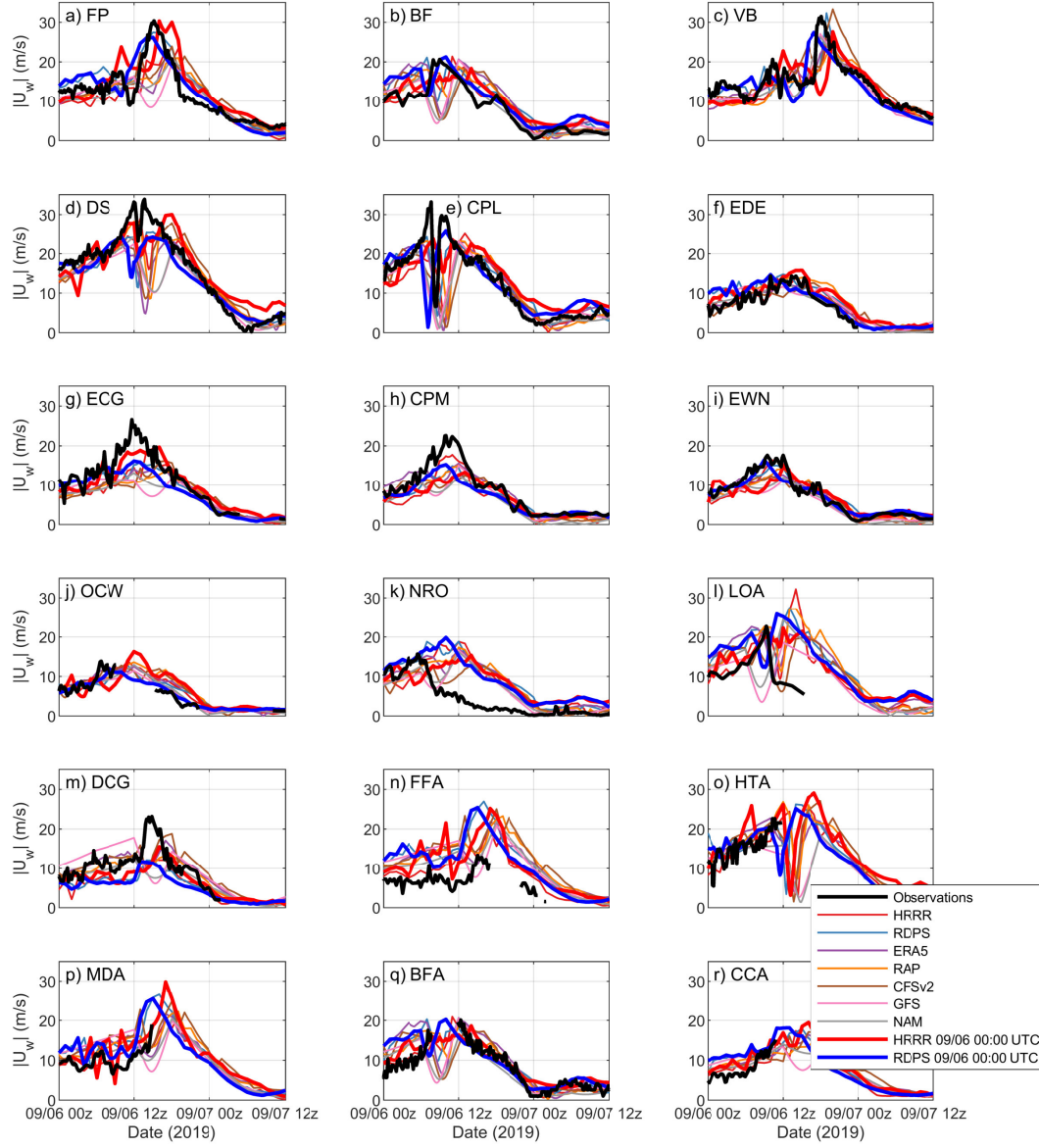


Figure A2: Observed, hindcasted, and forecasted wind magnitudes for 18 sites.

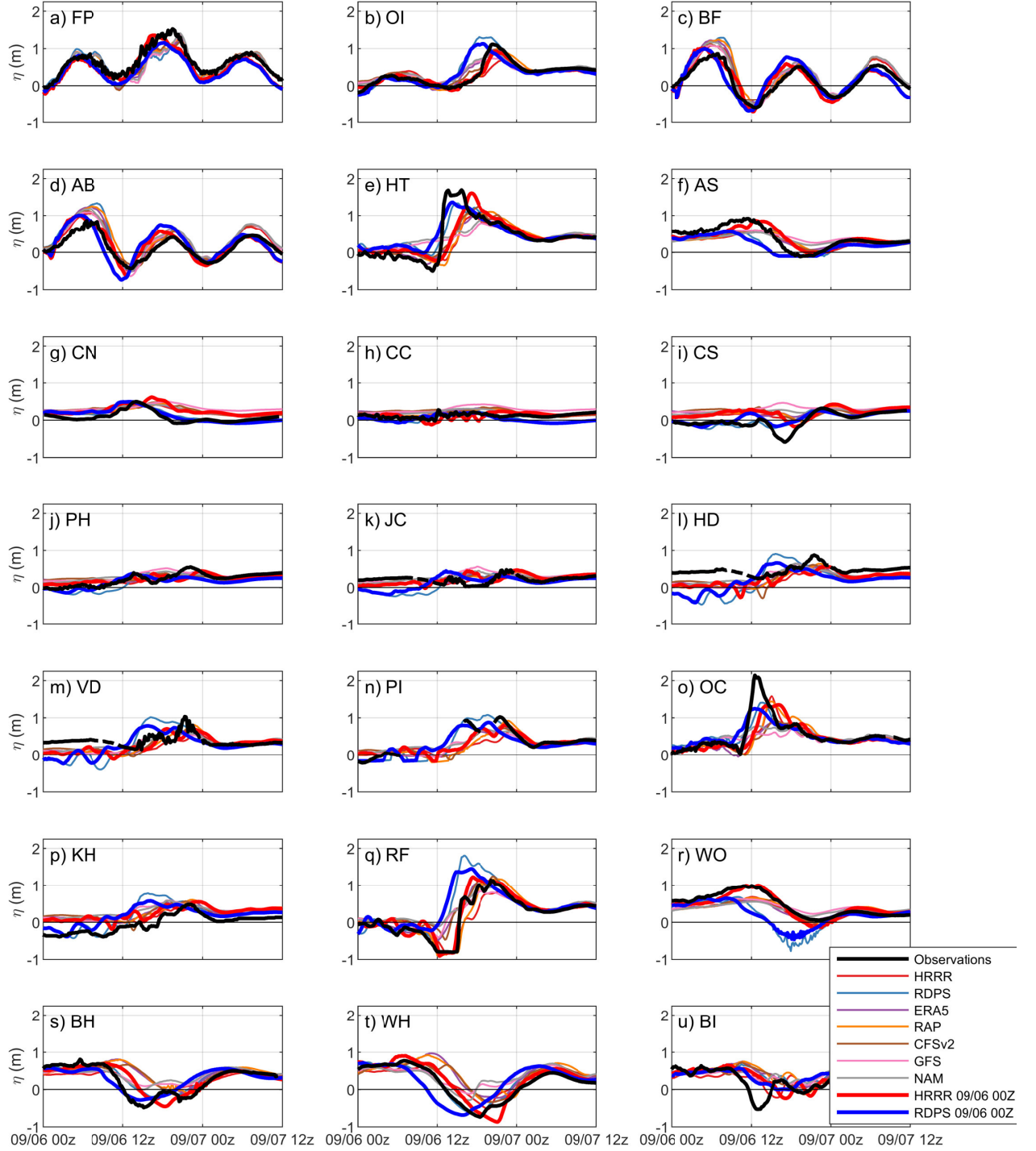


Figure A3: Observed, hindcasted, and forecasted water levels for 21 sites.

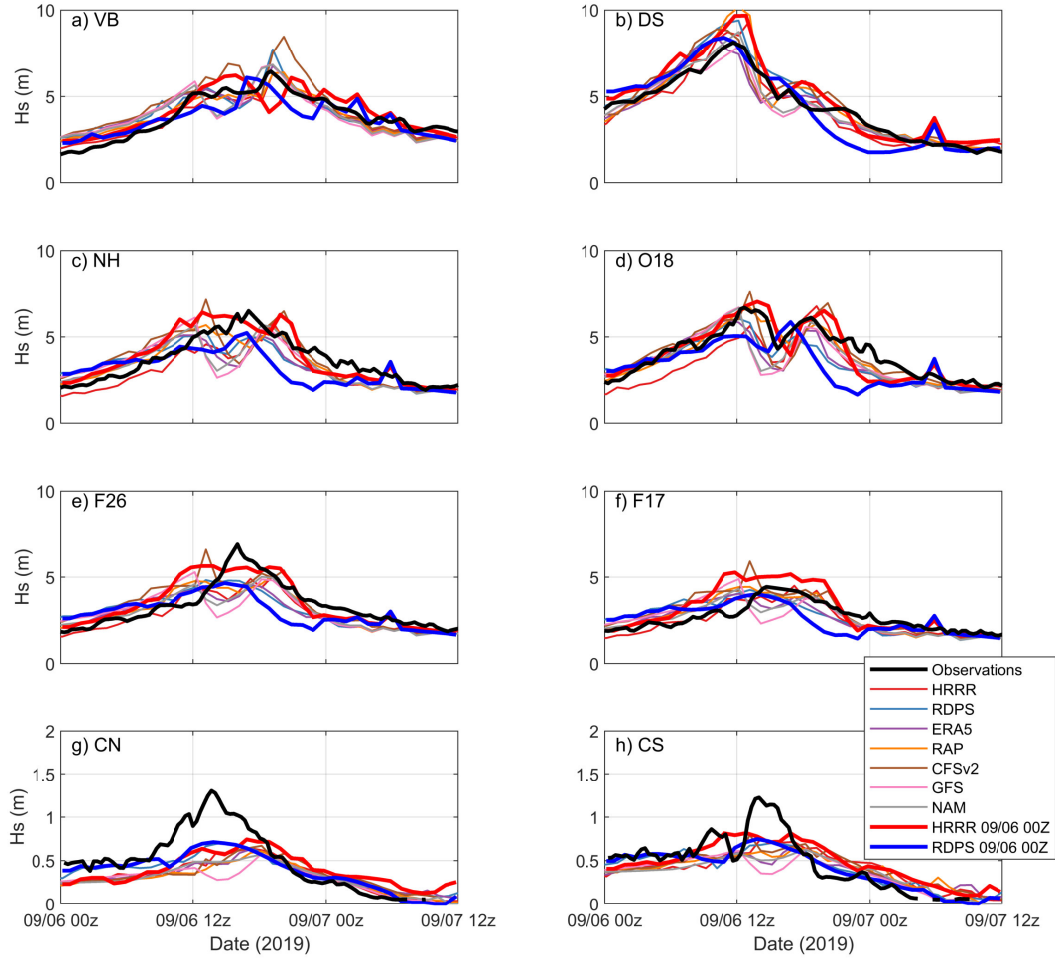


Figure A4: Observed, hindcasted, and forecasted significant wave heights for 8 sites. Note smaller scales in Currituck Sound compared to larger scale for ocean sites.

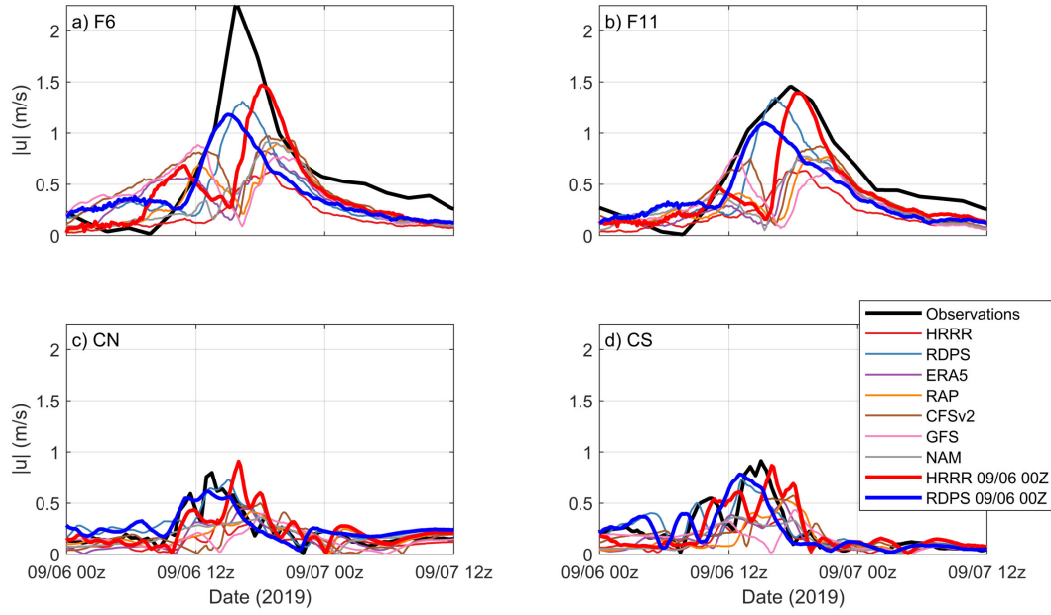


Figure A5: Observed, hindcasted, and forecasted depth averaged velocities at 4 sites.



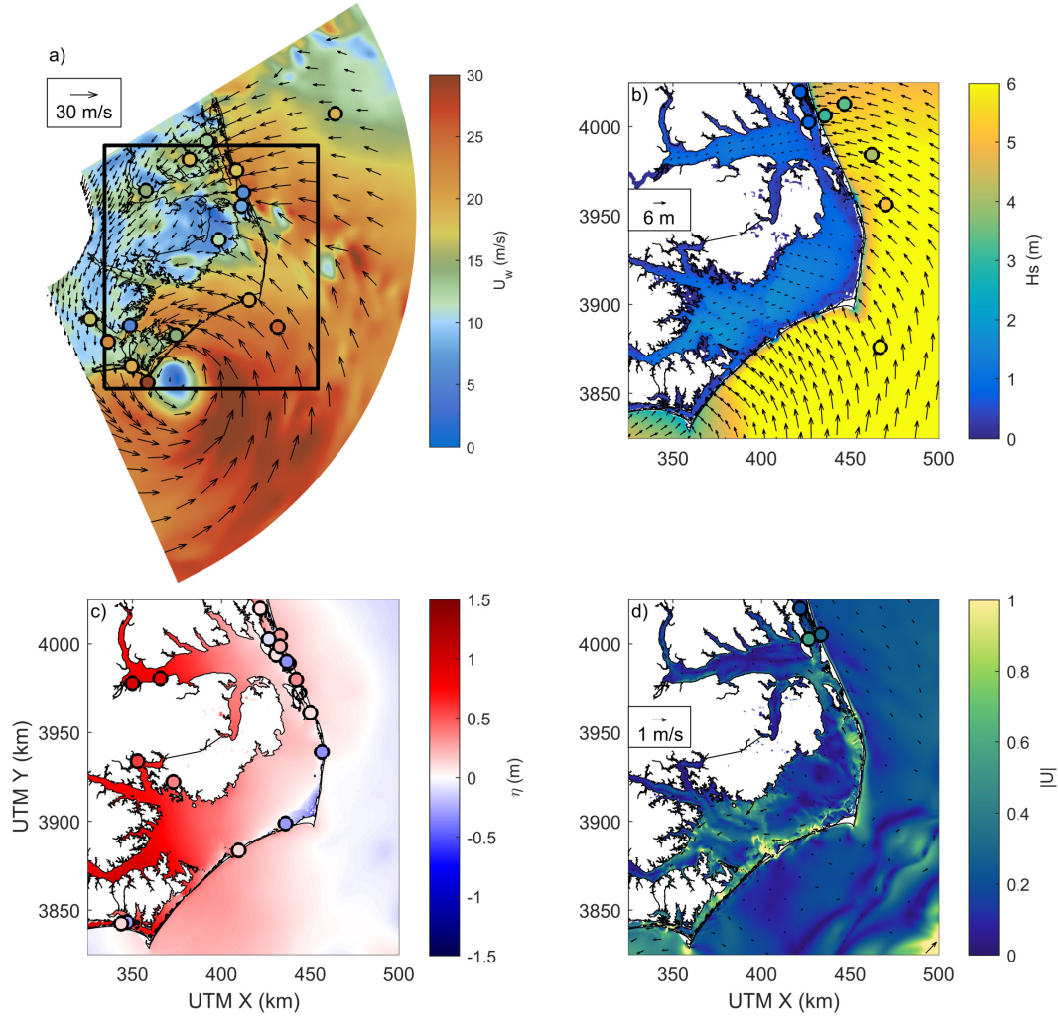


Figure A6: Example of model forcing and results on September 6, 2019 at 10:00 UTC: a) winds forecasted from the September 6 00:00 UTC HRRR model run; b) significant wave height; c) water levels; and d) depth-averaged currents. Observations are shown by coloured circles and model results are shown by the colour contours on the same scale.

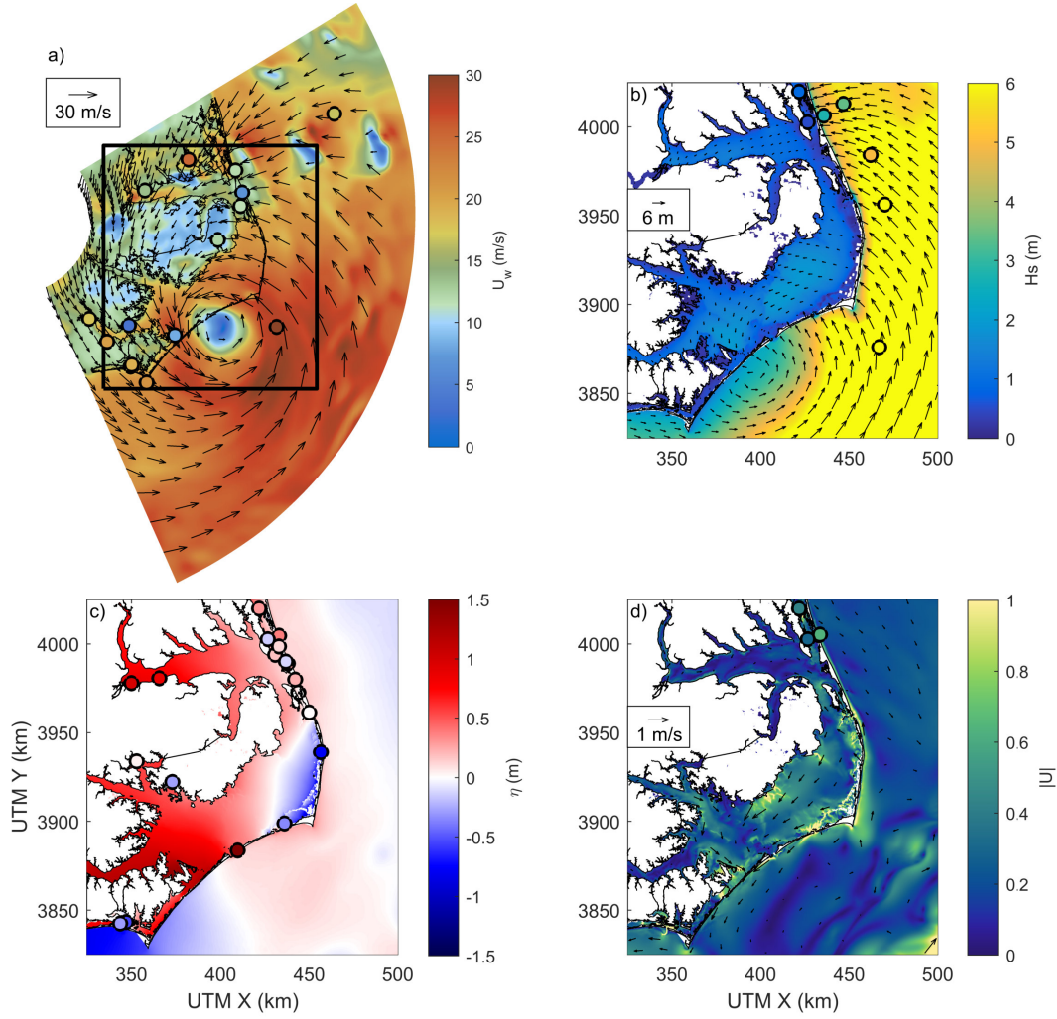


Figure A7: Example of model forcing and results on September 6, 2019 at 12:00 UTC: a) winds forecasted from the September 6 00:00 UTC HRRR model run; b) significant wave height; c) water levels; and d) depth-averaged currents. Observations are shown by coloured circles and model results are shown by the colour contours on the same scale.

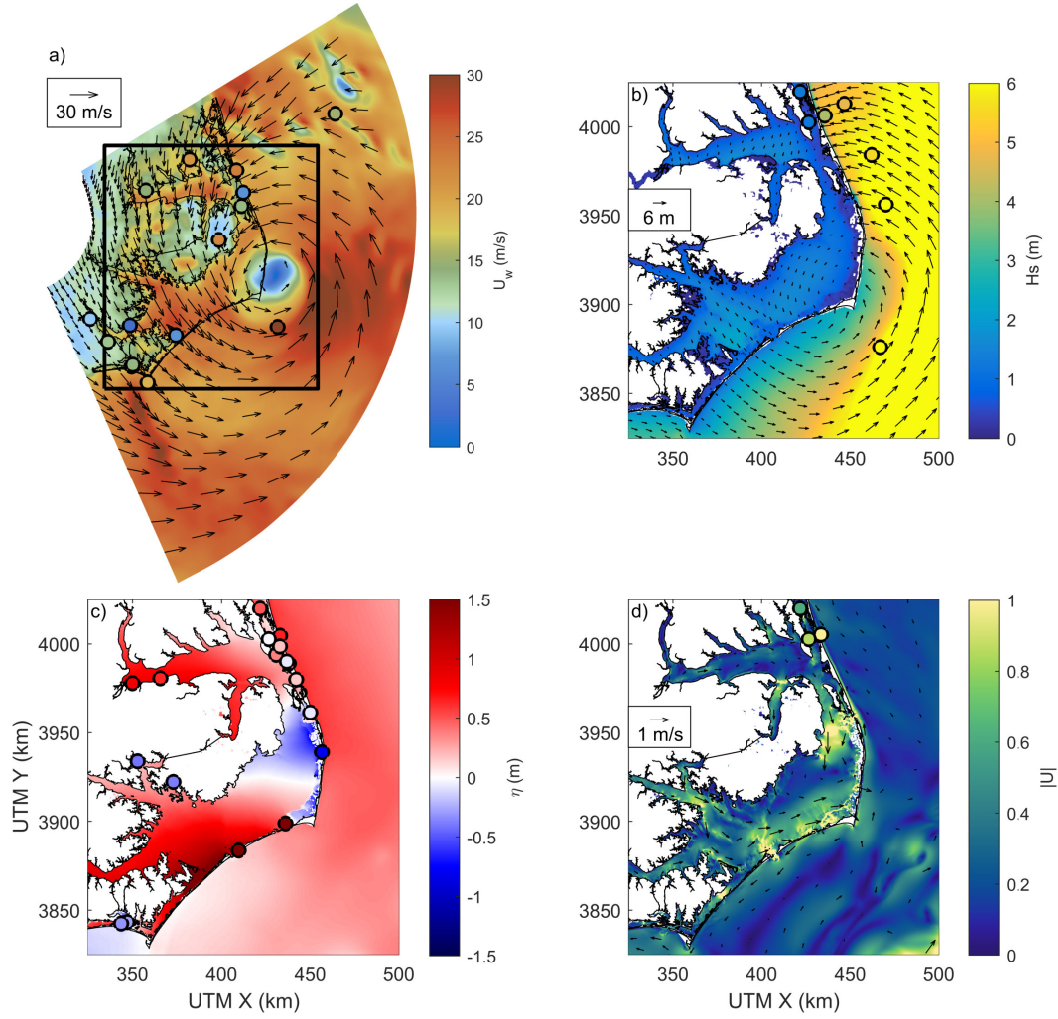


Figure A8: Example of model forcing and results on September 6, 2019 at 14:00 UTC: a) winds forecasted from the September 6 00:00 UTC HRRR model run; b) significant wave height; c) water levels; and d) depth-averaged currents. Observations are shown by coloured circles and model results are shown by the colour contours on the same scale

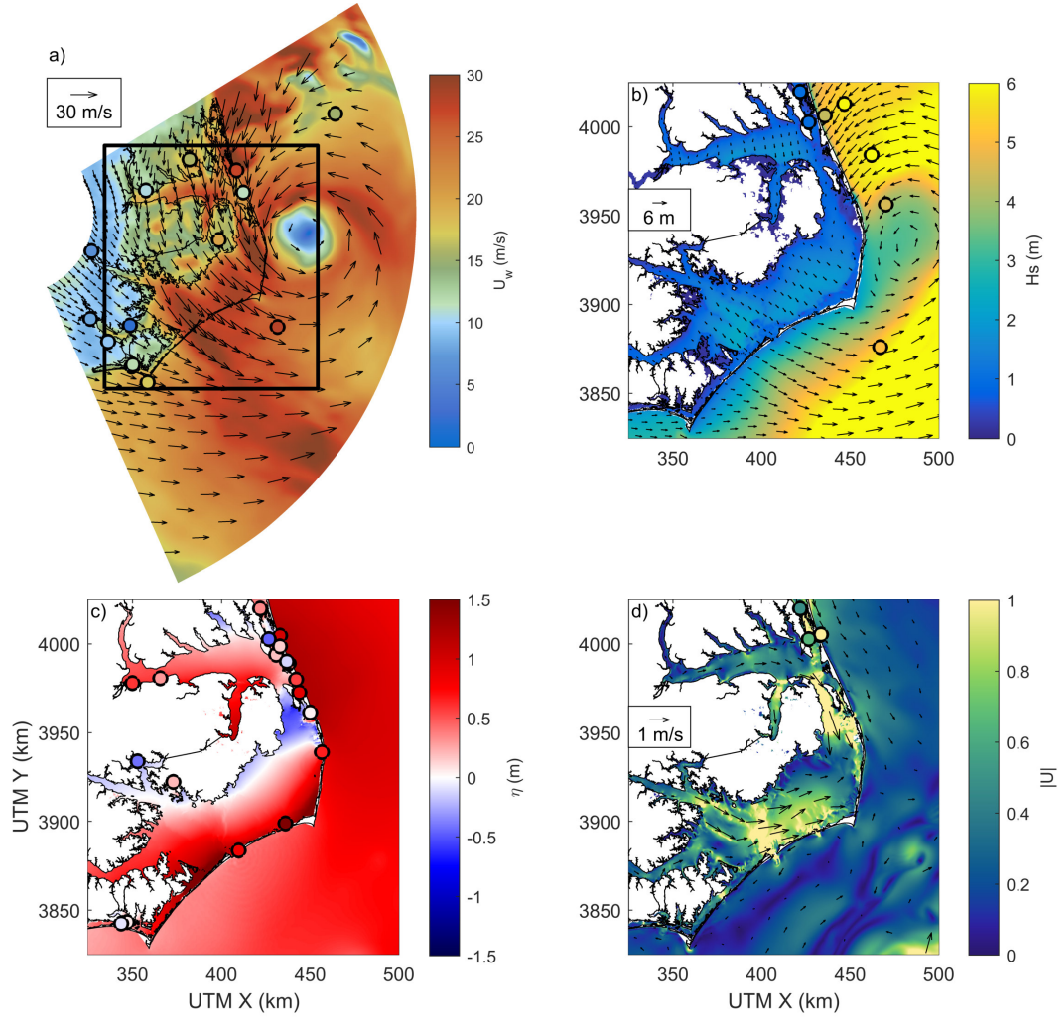


Figure A9: Example of model forcing and results on September 6, 2019 at 16:00 UTC: a) winds forecasted from the September 6 00:00 UTC HRRR model run; b) significant wave height; c) water levels; and d) depth-averaged currents. Observations are shown by coloured circles and model results are shown by the colour contours on the same scale.



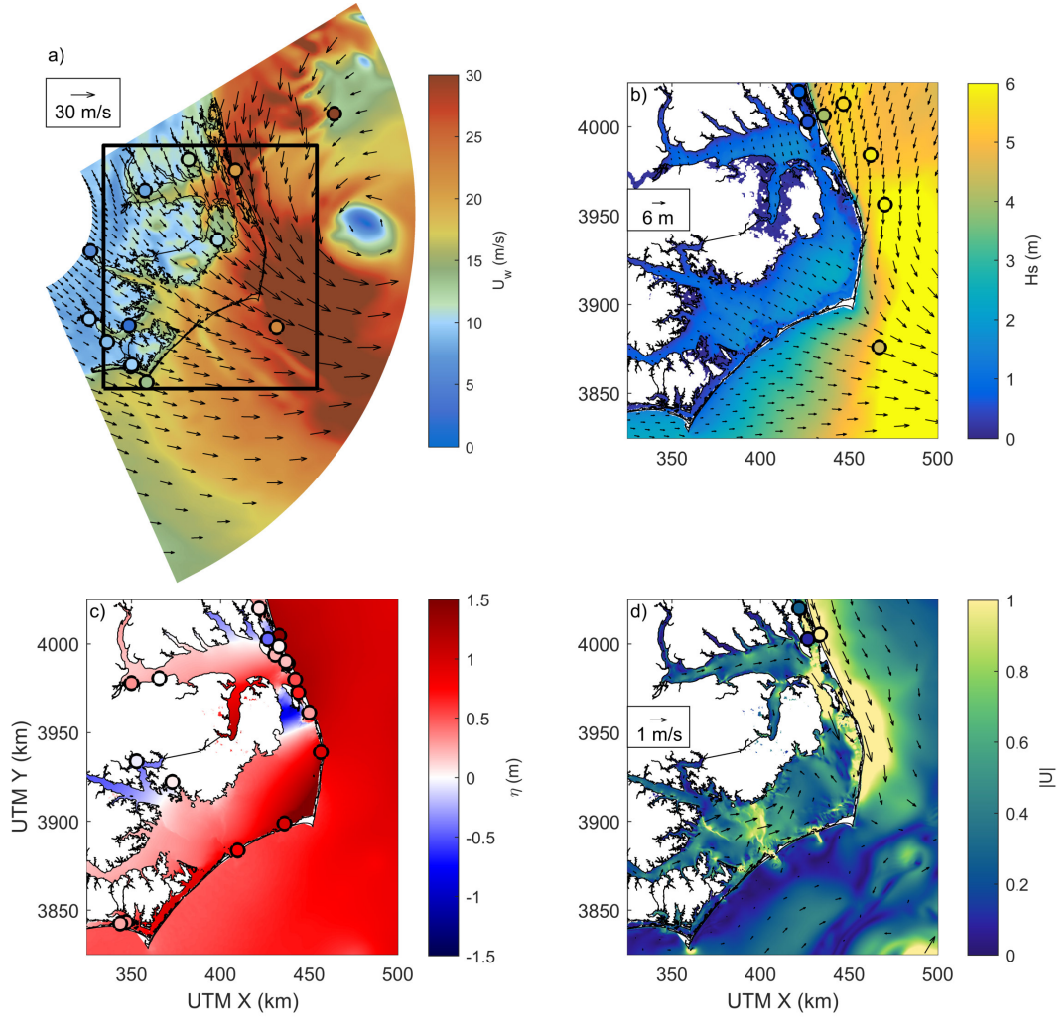


Figure A10: Example of model forcing and results on September 6, 2019 at 18:00 UTC: a) winds forecasted from the September 6 00:00 UTC HRRR model run; b) significant wave height; c) water levels; and d) depth-averaged currents. Observations are shown by coloured circles and model results are shown by the colour contours on the same scale.

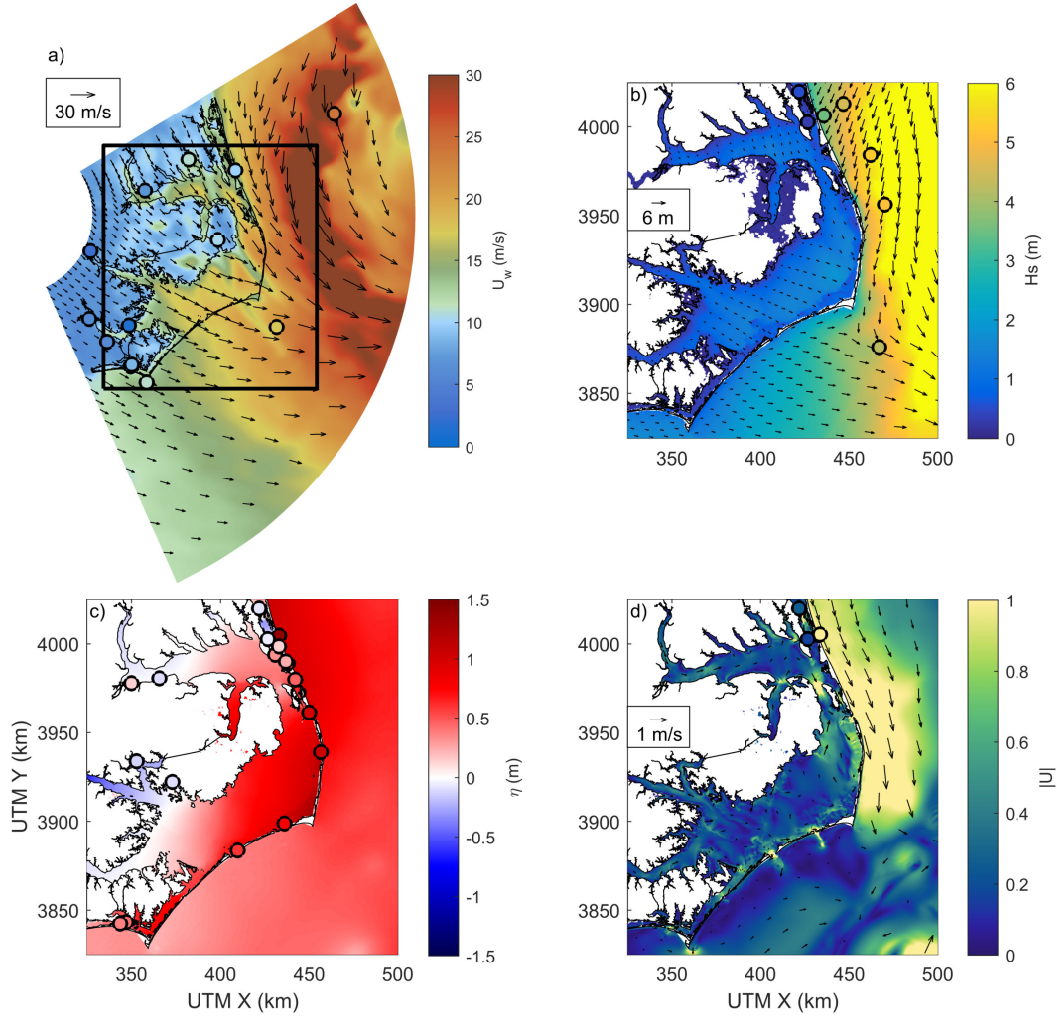


Figure A11: Example of model forcing and results on September 6, 2019 at 20:00 UTC: a) winds forecasted from the September 6 00:00 UTC HRRR model run; b) significant wave height; c) water levels; and d) depth-averaged currents. Observations are shown by coloured circles and model results are shown by the colour contours on the same scale.